Chapter 8

The Pacific Ocean

After these two lengthy excursions into polar oceanography we are now ready to test our understanding of ocean dynamics by looking at one of the three major ocean basins. The Pacific Ocean is not everyone's first choice for such an undertaking, mainly because the traditional industrialized nations border the Atlantic Ocean; and as science always follows economics and politics (Tomczak, 1980), the Atlantic Ocean has been investigated in far more detail than any other. However, if we want to take the summary of ocean dynamics and water mass structure developed in our first five chapters as a starting point, the Pacific Ocean is a much more logical candidate, since it comes closest to our hypothetical ocean which formed the basis of Figures 3.1 and 5.5. We therefore accept the lack of observational knowledge, particularly in the South Pacific Ocean, and see how our ideas of ocean dynamics can help us in interpreting what we know.

Bottom topography

The Pacific Ocean is the largest of all oceans. In the tropics it spans a zonal distance of 20,000 km from Malacca Strait to Panama. Its meridional extent between Bering Strait and Antarctica is over 15,000 km. With all its adjacent seas it covers an area of $178 \cdot 10^6$ km^2 and represents 40% of the surface area of the world ocean, equivalent to the area of all continents. Without its Southern Ocean part the Pacific Ocean still covers $147 \cdot 10^6$ km^2, about twice the area of the Indian Ocean.

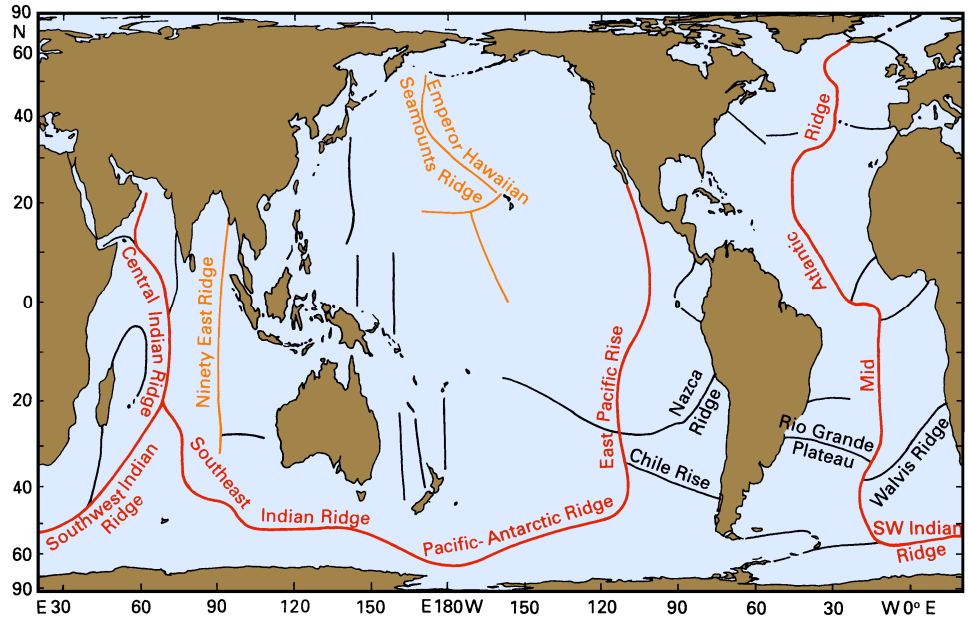

Fig. 8.1. The inter-oceanic ridge system of the world ocean (heavy line) and major secondary ridges. Structures with significant impact on ocean currents and properties are labelled.

All adjacent seas of the Pacific Ocean are grouped along its west coast. Some of them (such as the Arafura and East China Seas) are large shelf seas, others (e.g. the Solomon Sea) deep basins. In contrast to the situation in the Indian and Atlantic Oceans, adjacent seas of the Pacific Ocean exert little influence on the hydrology of the main ocean basins. The Australasian Mediterranean Sea, the only mediterranean sea of the Pacific Ocean, is a major region of water mass formation and an important element in the mass and heat budgets of the world ocean; but its influence on Pacific hydrology is of only minor importance, too, far less than its effect on the hydrology of the Indian Ocean.

Before considering the Pacific topography in detail it is worth looking at the world ocean as a whole. Figure 8.1 shows that a system of inter-oceanic ridges, the result of tectonic movement in the earth's crust, structures the world ocean into a series of deep basins. The major feature of this system is a continuous mountain chain that stretches from the Arctic Mediterranean Sea through the Atlantic and Indian Oceans into the Pacific Ocean and ends in the peninsula of Baja California. Numerous fracture zones cut deep into the slopes of this chain. To map them all in reliable detail will require an enormous amount of ship time and remains a task of the future. In the large-scale maps of this book the details cannot be shown anyway, but they are important where they connect deep basins which would otherwise be isolated. To give an idea of the real topography, Figure 8.2 gives an example of such a fracture zone from the Atlantic Ocean, on the original scale of the GEBCO charts. It is obvious that the world ocean has not been surveyed to that amount of detail and many passages for the flow of bottom water are not accurately known.

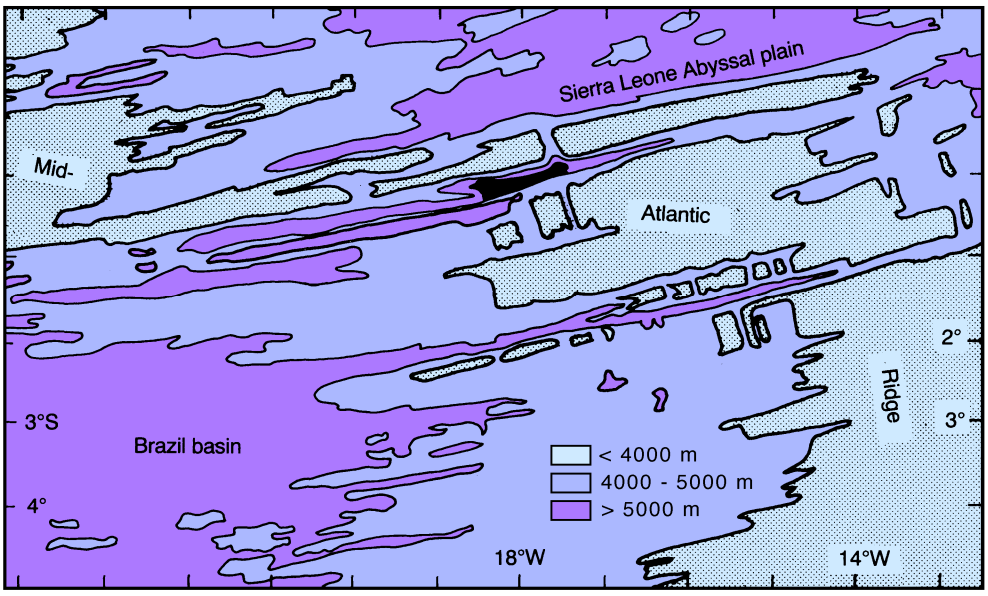

Fig. 8.2. An example of fracture zones in the inter-oceanic ridge system. the Mid-Atlantic Ridge at the equator. The ridge stretches from northwest to southeast as a series of depths <4000 m. It is cut by the Romanche Fracture Zone at the equator (identifiable by the Romanche Deep with depths >6000 m, shown in black) and the Chain Fracture Zone at 2° - 3°S. Two other fracture zones can be seen north of the equator. The figure is a simplified reproduction of part of a GEBCO chart, on the same scale.

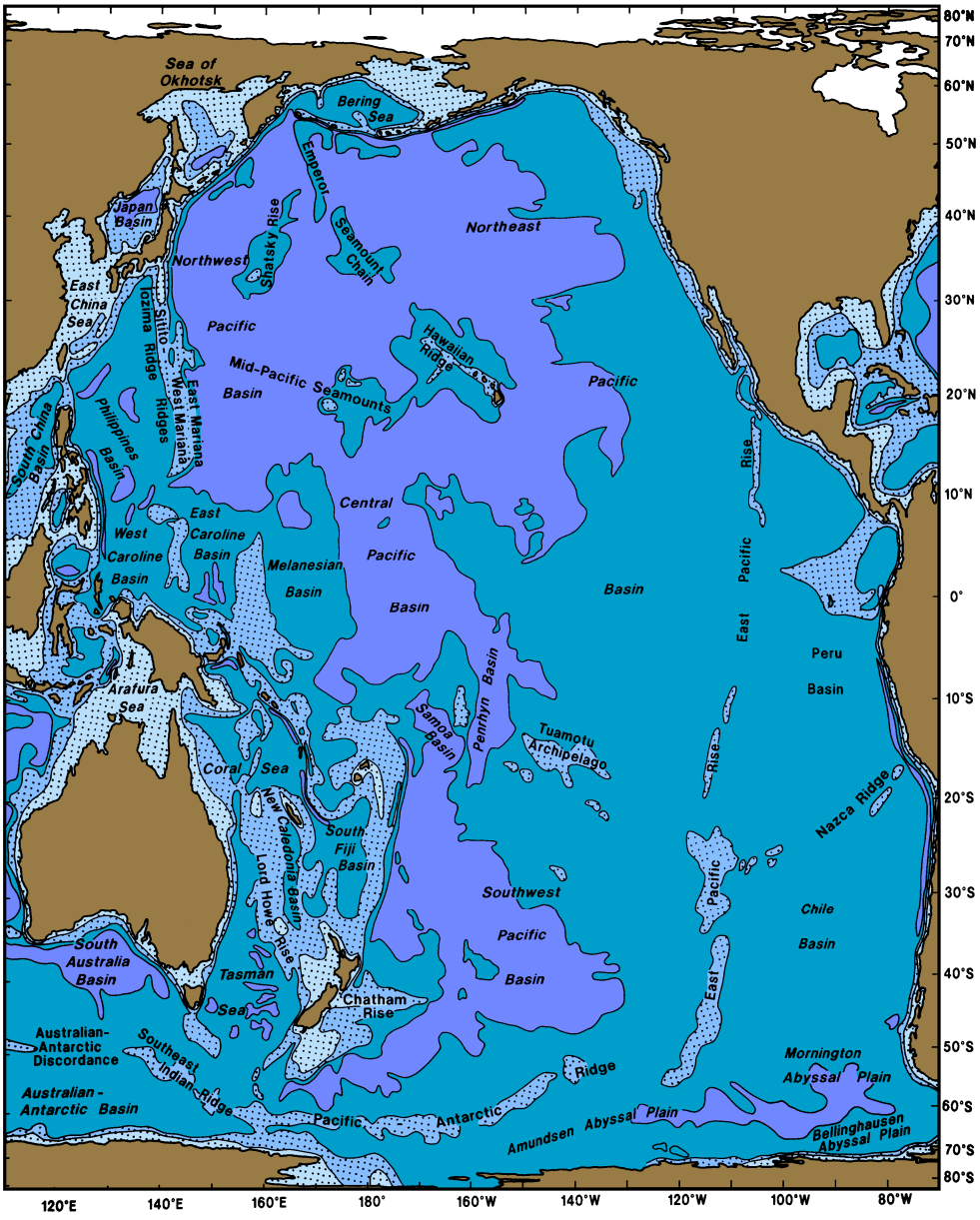

Fig. 8.3. Topography of the Pacific Ocean. The 1000, 3000, and 5000 m isobaths are shown, and regions less than 3000 m deep are shaded.

The inter-oceanic ridge system divides the Atlantic and Indian Oceans into compartments of roughly equal size. In the Pacific Ocean it runs close to the eastern boundary, producing divisions of the southeastern Pacific Ocean similar in size to the Atlantic and Indian basins. The vast expanse of deep ocean in the central and northern Pacific Ocean, on the other hand,

is subdivided more by convention than topography into the *Northeast Pacific, Northwest Pacific*, *Central Pacific*, and *Southwest Pacific Basins* (Figure 8.3). Further west, New Zealand and the Melanesian islands provide a natural boundary for two adjacent seas of the Pacific Ocean, the Tasman and Coral Seas, while in the north the *West* and *East Mariana Ridges* and the *Sitito-Iozima Ridge* offer a natural subdivision.

Communication between the Southern Ocean and the Pacific basins is much more restricted by the topography than in the other oceans. Flow of water from the Australian-Antarctic into the Southwest Pacific Basin and the Tasman Sea is blocked below the 3500 m level. Flow from the Amundsen Abyssal Plain into the Southwest Pacific Basin is possible to somewhat greater depth but not below 4000 m. The *Peru* and *Chile Basins* are closed to the north and west at the 3500 m level but connected with the *Mornington Abyssal Plain* and with each other at slightly greater depth, probably somewhere around 3600 - 3800 m.

A unique feature of the Pacific Ocean is its large number of seamounts, particularly in the Northwest and Central Pacific Basins. Seamounts are found in all oceans, but the volcanism of the northwestern Pacific Ocean produces them in such numbers that in some regions they cover a fair percentage of the ocean floor (Figure 8.4). This may have an impact on the dissipation of tidal energy. Their effect on mean water movement is probably negligible.

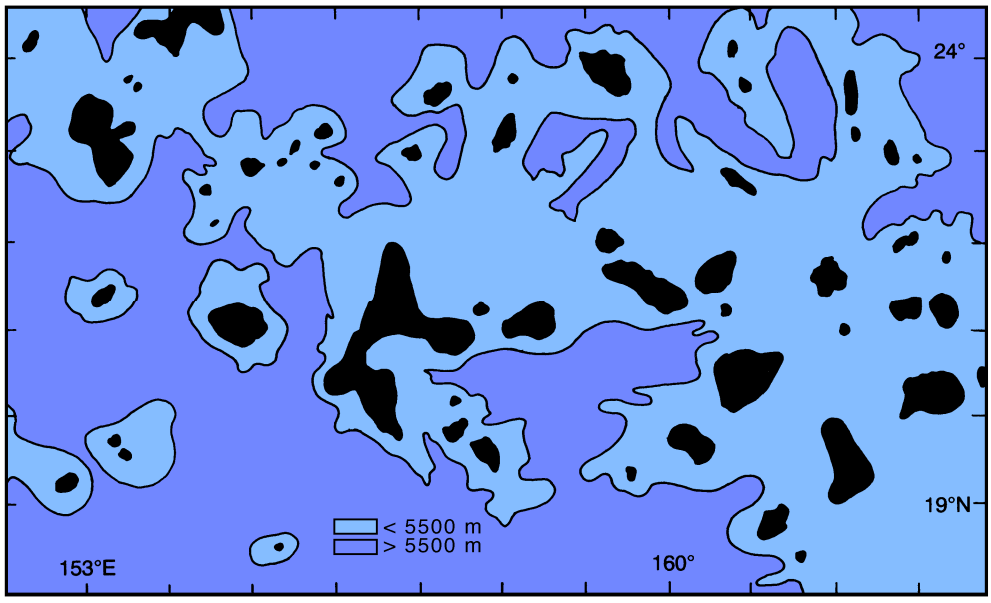

Fig. 8.4. Seamounts in the Northwest Pacific Basin. The 5500 m contour is shown, depths less than 3500 m are indicated in black. The peaks of most shallow structures are less than 2000 m below the sea surface; some of the larger structures may carry more than one peak. Simplified from a GEBCO chart and on the same scale.

The wind regime

The atmospheric circulation over the Pacific Ocean is shown in Figures 1.2 - 1.4. The northern Trades are the dominant feature in the annual mean. They are comparable in strength to the Trades in the Atlantic and southern Indian Ocean and make it difficult to see why the ocean received its reputation as the "pacific", or peaceful, ocean. The justification for the name is found in the southern hemisphere where east of 170°W the Trades are moderate or weak but extremely steady. Seasonal variations are also smaller south of the equator, since the belt of high pressure located at 28°S during winter is maintained during summer (January), pushed southward to 35°S by the heat low over the Australian continent, Papua New Guinea, and the Coral Sea. East of 170°W the distribution of air pressure changes little, and the Trades and Westerlies display correspondingly little seasonality there. The effect of the Australian summer low is felt west of 170°W; in the northern Coral Sea across to Vanuatu it produces a monsoonal wind pattern: during winter (June - September) the Trades provide southeasterly air flow, during summer (December - March) the North-west Monsoon blows from Papua New Guinea and Cape York.

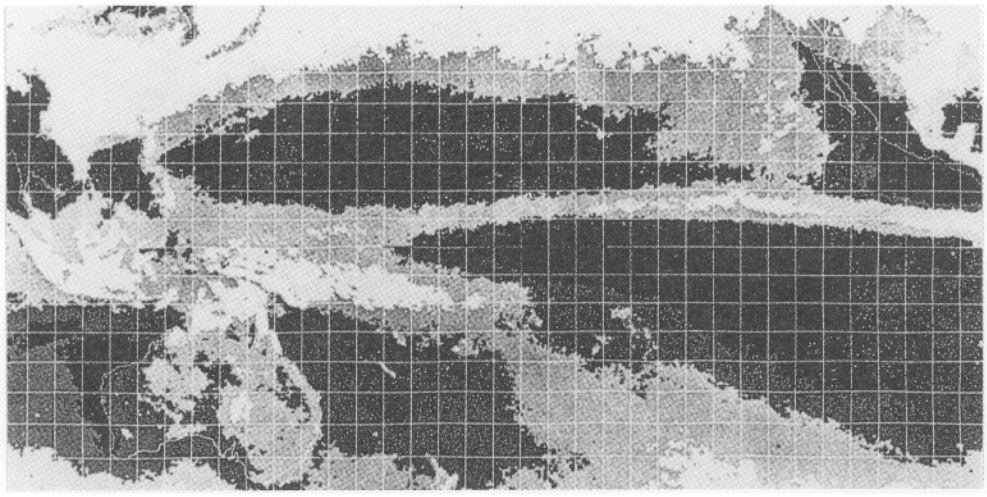

Fig. 8.5. The Intertropical Convergence Zone (ITCZ) and the South Pacific Convergence Zone (SPCZ) as seen in satellite cloud images. The figure is a composite of many months of observations, which makes the cloud bands come out more clearly. It covers the region 40°S - 40°N, 97°E - 87°W; the grid gives every 5° latitude and longitude.

The Trades and the Westerlies of both hemispheres are stronger in winter (July in the south, January in the north) than in summer. North of 55°N this is also true for the polar Easterlies which are barely noticeable in July but very strong in January when the Aleutian low and the Asian high are fully developed; the cyclonic winter circulation associated with the Aleutian low is so strong that it determines the annual mean. The Asian winter high extends a fair way over the ocean and produces a wind reversal over the East and South

China Seas and the region east of the Philippines; these regions thus experience monsoonal climate, with Northeast Monsoon during winter (December - March) and Southwest Monsoon during summer (June - September). The monsoon seasons and winds are the same as in the Indian Ocean, both monsoon systems being in fact elements of the same large seasonal wind system produced by the seasonal heating and cooling of the Asian land mass.

The Intertropical Convergence Zone (ITCZ) is located at 5°N, indicated by a minimum in wind speed (the Doldrums). A second atmospheric convergence known as the South Pacific Convergence Zone (SPCZ) extends from east of Papua New Guinea in a southeastward direction towards 120°W, 30°S. In the annual mean it is seen not so much as a wind speed minimum but more as a convergence in wind direction. Both convergences are regions of upward air movement and thus cloud formation. They are prominent features in satellite-derived maps of cloud cover (Figure 8.5) and will be addressed in more detail when their effect on rainfall and surface salinity is discussed in the following chapter. Contrary to widespread opinion, neither the ITCZ nor the SPCZ is a region of no wind; though winds are generally weak, completely calm conditions are encountered during not more then 30% of the year.

The integrated flow

We saw in Chapter 4 how the depth-integrated flow can be derived independently either from atmospheric or oceanic data. We now return to the relevant figures for a more detailed look at the situation in the Pacific Ocean.

Generally speaking, the integrated flow field derived from atmospheric data (Figure 4.4) compares well with the fields derived from oceanic data with different assumed depths of no motion (Figures 4.5 and 4.6). The most prominent feature is the strong subtropical gyre in the northern hemisphere, consisting of (Figure 8.6) the North Equatorial Current with strongest flow near 15°N, the Philippines Current, the Kuroshio, the North Pacific Current, and the California Current. The circulation in the subtropics of the southern hemisphere is weaker; but the gyre is again well resolved from both data sets. The high degree of agreement in the region of weak flow east of 160°W is particularly remarkable: flow away from the Circumpolar Current is northeastward south of 30°S, where it turns northwestward for a while before joining the general westward flow of the South Equatorial Current. This is one of the remotest regions of the world ocean - no shipping lanes pass through it, the distances to ports are too long for most research vessels to reach it, no islands offer refuelling facilities. This makes exploration of this part of the southern subtropical gyre an expensive undertaking. Until more information is obtained from drifting buoys and satellite data, the integrated flow field will remain our best information on currents in the region. Sverdrup dynamics should work particularly well there, and the flow pattern seen in Figures 4.4 - 4.7 should find confirmation from field observations.

More details are revealed in the stream function map (Figure 4.7). It shows the South Equatorial Current, centred around 15°S, and the Peru/Chile Current as major components of the southern subtropical gyre and indicates the existence of western boundary currents along the coasts of Australia and New Zealand. The split near 18°S into the southward flowing East Australian Current and northward flow in the Coral Sea and northward transport across the equator east of Papua New Guinea have been confirmed by recent field observations. The stream function map also reveals the existence of an Equatorial Counter-

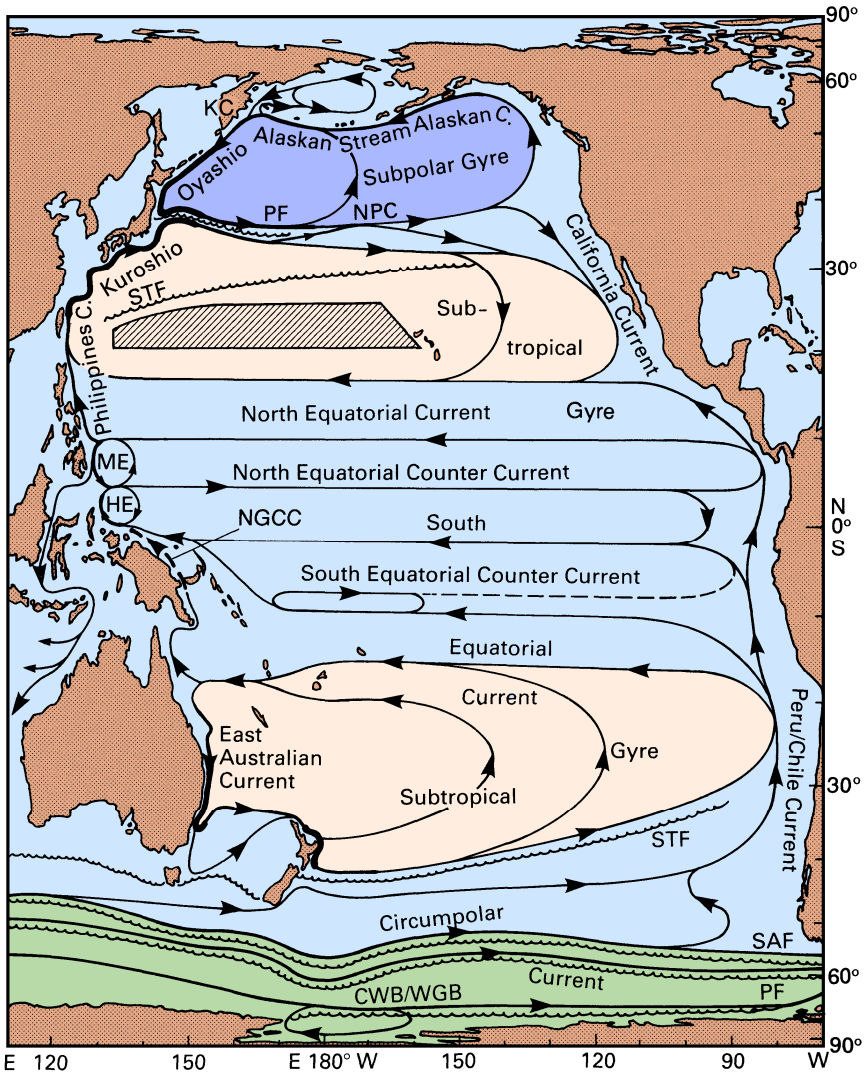

Fig. 8.6. Surface currents of the Pacific Ocean. Abbreviations are used for the Mindanao Eddy (ME), the Halmahera Eddy (HE), the New Guinea Coastal (NGCC), the North Pacific (NPC), and the Kamchatka Current (KC). Other abbreviations refer to fronts: NPC: North Pacific Current, STF: Subtropical Front, SAF: Subantarctic Front, PF: Polar Front, CWB/WGB: Continental Water Boundary / Weddell Gyre Boundary. The shaded region indicates banded structure (Subtropical Countercurrents). In the western South Pacific Ocean the currents are shown for April - November when the dominant winds are the Trades. During December - March the region is under the influence of the northwest monsoon, flow along the Australian coast north of 18°S and along New Guinea reverses, the Halmahera Eddy changes its sense of rotation and the South Equatorial Current joins the North Equatorial Countercurrent east of the eddy. Flow along the STF is now called the South Pacific Current (Stramma *et al.*, in press).

current near 5°N, fed from both subtropical gyres. The current's position coincides with that of the Doldrums, where it flows against the direction of the prevailing weak winds.

An indication of a subpolar gyre in the northern hemisphere is seen north of 50°N. Eastward transport in this gyre is again achieved by the North Pacific Current; the circulation is completed by the poleward and westward flowing Alaska Current, the Alaskan Stream, the southern part of the East Kamchatka Current, and the Oyashio.

In summary, the integrated flow indicates the presence of six western boundary currents: the southward flowing Oyashio between 60°N and about 45°N; the northward flowing Kuroshio between about 12°N and 45°N; the inshore edge of the Mindanao Eddy which flows southward from about 12°N to 5°N; a northward flowing unnamed current between 18°S and 5°N; the southward flowing East Australian Current between 18°S and Tasmania; and another southward current along the east coast of New Zealand. Compared to observations, the start and end latitudes for all boundary currents are quite accurate. An exception occurs in the case of New Zealand; observations show that the Tasman Current only travels to the south end of North Island, while a cold current flows northward along South Island. This may be the result of inadequacies in the wind data for the seldom-travelled region east of South Island.

A marked difference between the integrated flow fields derived from atmospheric and oceanic data is seen in the meridional gradients of integrated steric height just to the east of Japan (a similar phenomenon occurs in the north Atlantic Ocean). This difference does not reflect any inadequacy of the wind field; rather, it is a failure of Sverdrup dynamics which assumes broad, slow flow. The Oyashio and Kuroshio are neither broad nor slow, and they meet head-on off Japan. The Kuroshio advects warm water northward, causing steric height to be larger than it otherwise might be within the Kuroshio. Similarly, the Oyashio's advection of cold water reduces steric height below what we would expect from extending the Sverdrup relationship close to the western shore. Thus the gradient between the two is intensified, and the outflow from the two boundary currents is narrower and stronger than we would expect from the Sverdrup model. Narrow and strong flow (though still much broader than in reality) is indicated in Figures 4.5 and 4.6 which are based on oceanic observations averaged over many years. In contrast, the wind-based flow fields (Figures 4.4 and 4.7) spread the outflow unrealistically over more than 10 degrees of latitude.

The equatorial current system

When the structure of the circulation is investigated in detail it is found that significant elements of the current field do not show up clearly in the vertically integrated flow. Details of the three-dimensional structure are revealed in field observations, which we shall now review. We divide the discussion into the three major components of the circulation, the equatorial, western boundary, and eastern boundary currents, and begin with the equatorial current system.

Figure 8.7 is a schematic summary of the various elements of the equatorial current system in the Pacific Ocean. It is seen that the system has a banded structure and contains more elements of eastward flow than could be anticipated from the integrated flow field, which indicated only the presence of the North Equatorial Countercurrent. The most prominent of all eastward flows is the *Equatorial Undercurrent* (EUC). It is a swift flowing ribbon of water extending over a distance of more than 14,000 km along the equator with a thickness of only 200 m and a width of at most 400 km. The current core is found at

200 m depth in the west, rises to 40 m or less in the east and shows typical speeds of up to 1.5 m s^{-1}. Surface flow above the EUC is usually to the west, and the EUC does not appear in reports of ship drift. Although it is the swiftest of all equatorial currents its existence remained unknown to oceanographers until 1952 when it was discovered by Townsend Cromwell and Ray Montgomery. None of the theories of ocean dynamics at the time predicted eastward subsurface flow at the equator. The discovery of the Atlantic Equatorial Undercurrent by Buchanan 80 years earlier (see Chapter 14) had been forgotten, and the discovery of the Pacific EUC was therefore a major event in oceanography; for a few years after Cromwell's death the Undercurrent was called the Cromwell Current.

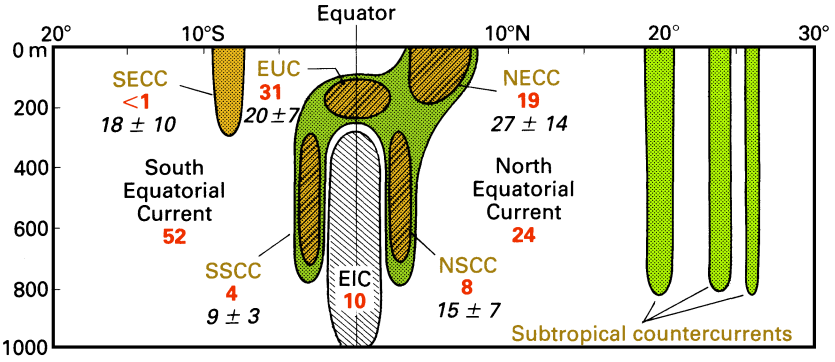

Fig. 8.7. A sketch of the structure of the equatorial current system in the central Pacific Ocean (170°W). Eastward flow is coloured. All westward flow north of 5°N constitutes the North Equatorial Current, westward flow south of 5°N outside the EIC represents the South Equatorial Current. EUC = Equatorial Undercurrent, EIC = Equatorial Intermediate Current, NECC and SECC = North and South Equatorial Countercurrents, NSCC and SSCC = North and South Subsurface Countercurrents. Transports in Sverdrups are given for 155°W (bold figures; based on observations from April 1979 - March 1980) and 165°E (italics, based on January 1984 - June 1986).

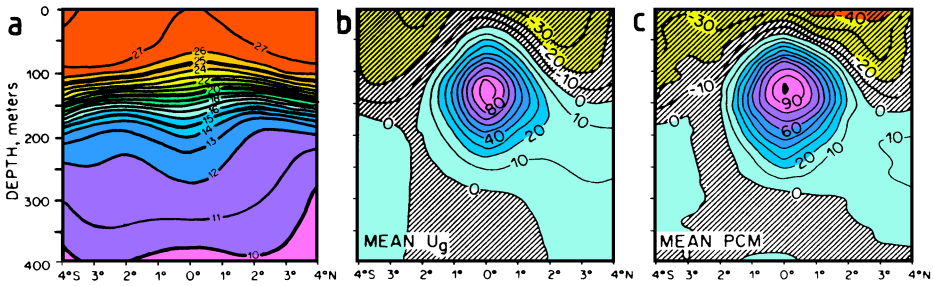

Fig. 8.8. The Equatorial Undercurrent during February 1979 - June 1980 near 155°W. (a) Mean temperature (°C), (b) mean geostrophic zonal velocity (10^{-2} m s^{-1})X, (c) mean observed zonal velocity (10^{-2} m s^{-1}). Note the spreading of the isotherms at the equator. From Lukas and Firing (1984).

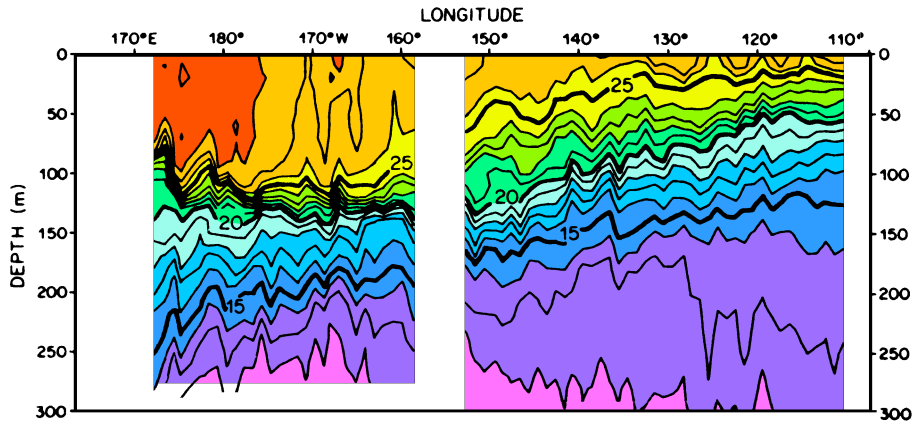

Fig. 8.9. A hydrographic section along the equator. Note the variation in the thickness of the nearly isothermal layer (temperatures above 26°C) from 100 m in the west to less than 20 m in the east, and the upward slope of the thermocline (temperatures between 15°C and 20°C) from west to east from 200 m to 70 m. From Halpern (1980).

In hydrographic sections the EUC is seen as a spreading of the isotherms in the thermocline (Figure 8.8). This weakening of the vertical temperature gradient occurs for two reasons. Firstly, it shows the "thermal wind" character of the Undercurrent (rule 2a in Chapter 3): above about 150 m, eastward current *increases* with depth, and isotherms slope downward on either side of the current; between 150 m and 250 m, eastward current *decreases* with depth, and isotherms slope upward. A second reason becomes apparent when we look at the processes that drive the Undercurrent. We noted in Chapter 3 that at the equator geostrophy works only for zonal flow. This is indeed shown by the fact that the thermal wind equation holds for the Undercurrent, i.e. the *meridional* component of the pressure gradient (indicated by the north-south slope of the isotherms) is in geostrophic balance. But the pressure gradient at the equator also has a *zonal* component, a result of the Trades which dominate the tropics and subtropics from 30°S to 30°N and produce an accumulation of warm water in the western Pacific Ocean. The accumulation of water is evident in any hydrographic section along the equator as a downward slope of the thermocline towards the west (Figure 8.9); according to our rule 1a this indicates a westward rise of the sea surface. The sea level difference between the Philippines and Central America amounts to about 0.5 m and produces a zonal pressure gradient which is unopposed by a Coriolis force. As a result, the current below the wind-driven surface layer accelerates down the pressure gradient (i.e. from west to east) until friction between the current and its surroundings prevents further acceleration of the flow and establishes a steady state. Friction is associated with mixing, and the Equatorial Undercurrent is therefore a region of unusually strong mixing. This leads to a weakening of the gradients normally found in the thermocline and contributes to the observed spreading of isotherms.

Recent observations indicate that in the depth range of the western Pacific thermocline, exchange between the northern and southern subtropical circulation systems is very limited, the separation between the two being located at the southern flank of the North Equatorial

Countercurrent. Evidence for strong separation is found in the T-S characteristics. Figure 8.10 shows T-S curves from the region north of Papua New Guinea. The change from high salinity water of southern origin to low salinity northern water occurs within 250 km between 1°S and 2°N. That this separation of the circulation is maintained towards the east is seen in the distribution of tritium introduced into the ocean from atmospheric bomb tests during the late 1950s and early 1960s. These tests were all performed in the northern hemisphere; tritium entered the thermocline through subduction at the northern Subtropical Convergence and quickly reached the equatorial current system. In 1973 - 1974 tritium levels surpassed 4 TU (1 TU = 1 tritium atom per 10^{18} hydrogen atoms) north of 3°N and had reached 9 TU near 12°N. In comparison, tritium values south of 3°N were close to 1.5 TU (Fine *et al.*, 1987).

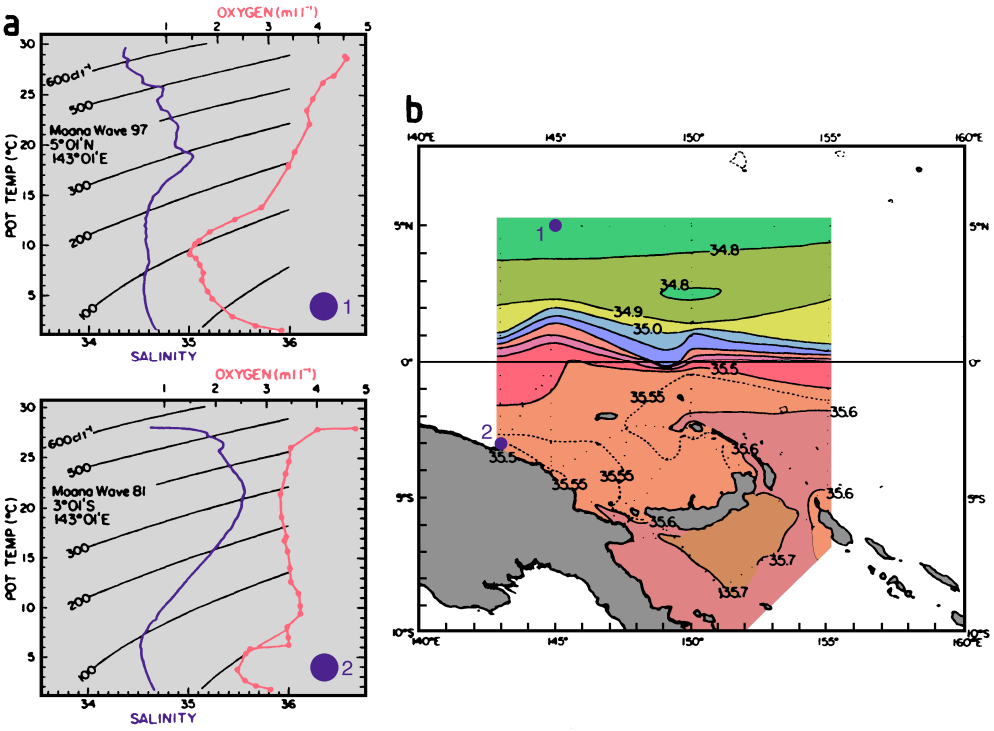

Fig. 8.10. Evidence for separation between northern and southern hemisphere circulation systems in the Pacific thermocline. (a) T-S diagrams and T-O_2 diagrams (identified by circles) from two stations north of Papua New Guinea, (b) salinity on an isopycnal surface located at approximately 180 m depth. Note the difference in maximum salinity and the crowding of the isohalines between the equator and 3°N. From Tsuchiya *et al.* (1989).

From the location of the separation zone north of the equator it can be concluded that the Equatorial Undercurrent belongs entirely to the southern circulation system. Observations show that its source waters originate nearly exclusively from the southern hemisphere. Most of the 8 Sv transported by the EUC past 143°E can be traced back to the South

Equatorial Current (Figure 8.11). The transport of the EUC increases downstream, reaching 35 - 40 Sv in the east. Based on the tritium distribution it must be assumed that the water drawn into the EUC along its way also stems mainly from the south. The southern origin of its waters allows the EUC to be identified as a subsurface salinity maximum. Figure 8.12 shows seasonal mean T-S diagrams from the termination region of the Undercurrent. The seasonal variation of salinity at temperatures above 13°C indicates that the EUC flows strongest during January - June but is much weaker in July - December.

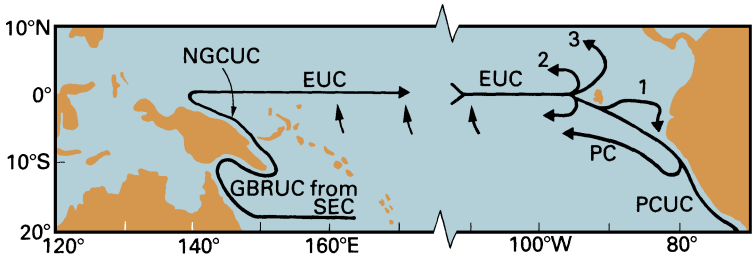

Fig. 8.11. The path of the Equatorial Undercurrent (EUC). SEC: South Equatorial Current. GBRUC: Great Barrier Reef Undercurrent. NGCUC: New Guinea Coastal Undercurrent. PCUC: Peru/Chile Undercurrent. PC: Peru Current (extends to the surface). Flow along path (1) does not occur during July-November. Path (2) is a contribution to the northern flank of the South Equatorial Current, path (3) a smaller contribution to the North Equatorial Current. Based on Tsuchiya *et al.* (1989) and Lukas (1986).

The second most important eastward flow in the equatorial current system is the *North Equatorial Countercurrent* (NECC). It is prominent in the integrated flow which shows it being fed by western boundary currents both from the south and the north (Figure 4.7). Its annual mean transport decreases uniformly with longitude, from 45 Sv west of 135°E to 10 Sv east of the Galapagos Islands. In its formation region the NECC participates in the Mindanao Eddy. At its other end it turns north on approaching the central American shelf, creating cyclonic flow close to the continent. According to rule 2 of Chapter 3 cyclonic motion is associated with a rise of the thermocline in its centre. In the termination region of the NECC this effect is known as the Costa Rica Dome, a minimum in thermocline depth near 9°N, 88°E (Figure 8.13).

The NECC varies seasonally in strength and position. During February - April when the Northwest Monsoon prevents the South Equatorial Current from feeding the NECC (see below) the Countercurrent is fed only from the north. It is then restricted to 4 - 6°N with a volume transport of 15 Sv and maximum speeds below 0.2 m s^{-1}; east of 110°W it disappears altogether. During May - January the NECC flows between 5°N and 10°N with surface speeds of 0.4 - 0.6 m s^{-1}. It is then fed from both hemispheres, a fact somewhat at odds with the tritium data west of the dateline, which place the separation zone between the circulation of the hemispheres to the south of the NECC and indicate little NECC contact with the southern circulation. The likely answer is that the water that enters the NECC west of 140°E from the south is again lost to the south before reaching the dateline.

Significant loss of water from the current is indicated by the strong eastward decrease of its transport. Historical data indicate that in the eastern Pacific Ocean most of this loss occurs to the south.

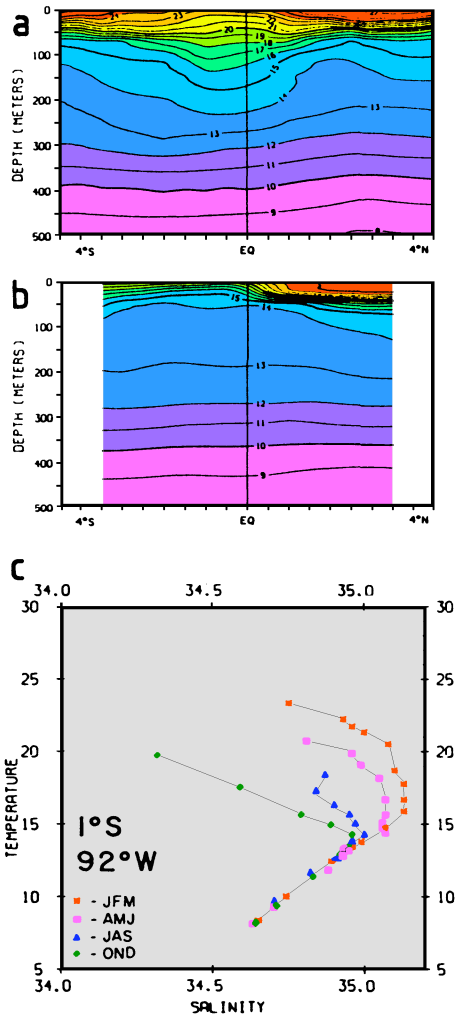

Fig. 8.12 (left). Seasonal variability of the Equatorial Undercurrent in the termination region at 92°W.
(a) Mean temperature (°C) for January - March,
(b) mean temperature (°C) for October - December,
(c) seasonal mean T-S curves. Low salinity and the absence of isotherm spreading in October - December indicate the absence of the Undercurrent. From Lukas (1986).

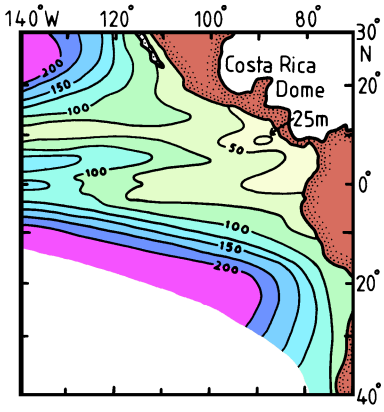

Fig. 8.13. Annual mean depth of the thermocline in the eastern Pacific Ocean, showing the Costa Rica Dome. After Voituriez (1981).

The major westward components of the equatorial current system are the *North Equatorial Current* (NEC) and the *South Equatorial Current* (SEC). Both are directly wind-driven and respond quickly to variations in the wind field. They are therefore strongly seasonal and reach their greatest strength during the winter of their respective hemispheres when the Trades are strongest. The NEC carries about 45 Sv with speeds of 0.3 m s^{-1} or less; it is strongest in February. The SEC is strongest in August when it reaches speeds of 0.6 m s^{-1}. Its transport at the longitude of Hawaii (155°W) is then about 27 Sv; this

decreases to 7 Sv in February. In the eastern Pacific Ocean between 110°W and 140°W horizontal shear between the SEC and the NECC is so large that wave-shaped instabilities develop along the separation zone between the two currents. They are seen as fluctuations of the meridional velocity component and steric height with periods of 20 - 25 days and wavelengths of 1000 km; satellite observations of sea surface temperature show them as cusped waves along the temperature front between the two currents (Figure 8.14). The instability disappears during March - May when the SEC and NECC flow with reduced strength.

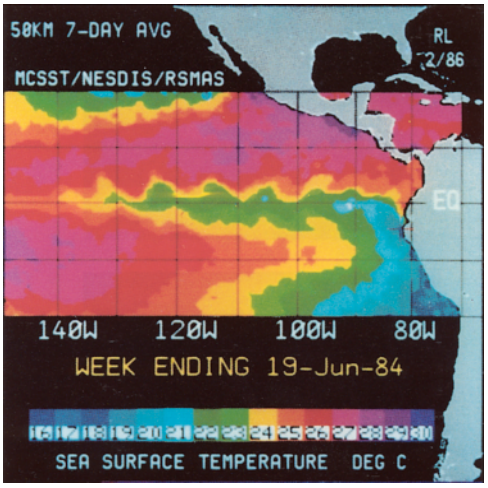

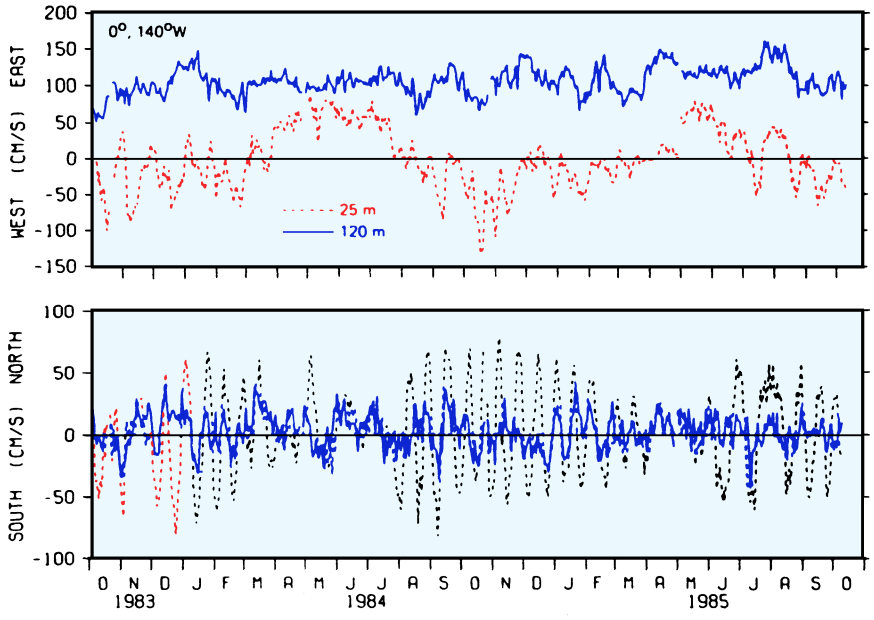

Fig. 8.14. Instabilities at the front between the South Equatorial Current and the North Equatorial Countercurrent in the eastern Pacific Ocean.
(a, left) Satellite image of sea surface temperature in the eastern equatorial Pacific Ocean showing cool water along the equator resulting from upwelling and waves of about 1000 km wavelength in the region of the largest gradient. From Legeckis (1986)
(b, below) Daily means of current components at the equator, 140°W. Note that the 20 - 25 day oscillations do not occur in the Equatorial Undercurrent (120 m level) and are restricted to the meridional component. Note also the absence of oscillations during March - June. From Halpern *et al.* (1988).

On approaching Australia the South Equatorial Current bifurcates near 18°S; part of it feeds the East Australian Current, while its northern part continues northward along the Great Barrier Reef and through the Solomon Sea and passes through Vitiaz Strait to feed the North Equatorial Countercurrent and the Euqatorial Undercurrent. This northern path is suppressed near the surface during the Northwest Monsoon season (December - March) but continues below the then prevailing southward surface flow as the Great Barrier Reef Undercurrent (Figure 8.11). The SEC therefore continues to feed the Equatorial Undercurrent during the monsoon season but does not supply source waters for the North Equatorial Countercurrent during those months.

The *Equatorial Intermediate Current* (EIC) is an intensification of westward flow within the general westward movement of the SEC. Observations over 30 months at 165°E gave an average westward transport of 7.0 ± 4.8 Sv with speeds above 0.2 m s^{-1} near 300 m. At 150 - 160°W its core is consistently found with speeds above 0.1 m s^{-1} near 900 m. At the same latitudes the cores of the *South Subsurface Countercurrent* and the *North Subsurface Countercurrent* are usually located near 600 m. An explanation for the existence of these currents is still lacking. Recent observations indicate that the banded structure of currents at the equator continues to great depth (Figure 8.15). Below the permanent thermocline currents exceeding 0.2 m s^{-1} are quite rare in the open ocean, and the existence of such currents near the equator indicates that the dynamics of the equatorial region cannot be explained by our $1^1/_2$ layer model. The EIC, NSCC, and SSCC are integral parts of a dynamic system that reaches much deeper than the thermocline. The fact that the Costa Rica Dome is a permanent feature despite strong seasonality of the North Equatorial Countercurrent indicates that the NSCC also plays a part in maintaining the thermocline structure in the Dome.

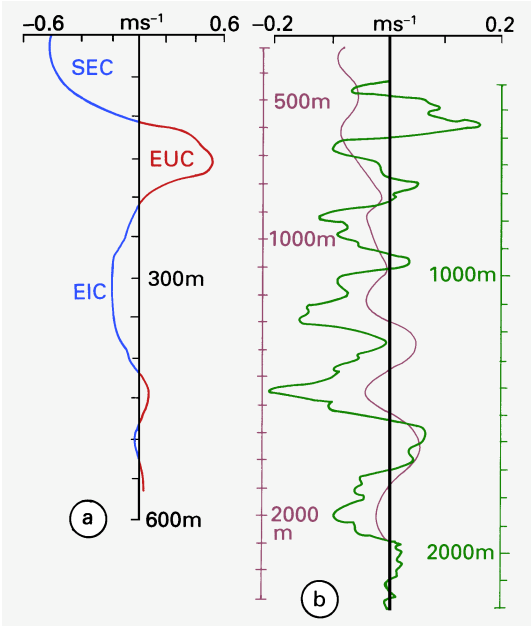

Fig. 8.15. Evidence for banded structure of currents at the equator.
(a) The South Equatorial Current (SEC), Equatorial Undercurrent (EUC), and Equatorial Intermediate Current (EIC) at 165°E;
(b) deep equatorial currents at 150 - 160°W during 1980 (solid line, right depth scale) and during March 1982 - June 1983 (thin line, left depth scale). The cores of all current bands coincide if the entire current system during 1982/83 is shifted upward some 130 m.
Note the different depth and velocity scales. Adapted from Delcroix and Henin (1988) and Firing (1987).

The *South Equatorial Countercurrent* is a weak eastward surface current not seen in current maps based on ship drifts but persistently found in results of geostrophic calculations. This may be due to lack of ship traffic, high variability in space and time, or both. Typical surface speeds are below 0.3 m s^{-1} at 170°E, giving a transport of about 10 Sv. Like its northern counterpart the stronger NECC, it is located at a minimum of annual mean wind stress and is therefore strongly seasonal. It is strongest during the Northwest Monsoon (the cause of the wind stress minimum, February - April) and barely seen during winter. In both seasons its strength decreases rapidly east of the dateline (see Figure 8.6), and it may be absent from the eastern Pacific Ocean during most months.

Superimposed on the zonal circulation of Figure 8.6 is weak but important meridional movement. The most important element is at the equator where the Ekman transport in the South Equatorial Current is to the right in the northern hemisphere and to the left in the southern hemisphere. This produces a surface divergence and *equatorial upwelling* in the upper 200 m of the water column. The resulting vertical movement can be determined only by indirect means. Using an array of current meter moorings and applying the principle of continuity of mass between diverging flows it has been estimated as of the order of 0.02 m per day. This is about one order of magnitude smaller than vertical movement in coastal upwelling regions, but the effect is clearly seen in the sea surface temperature (Figures 2.5a and 8.14a). Observations of tritium near the equator are consistent with a vertical transport of 47 Sv, indicating that upwelling is an important element of the current system. The meridional motion associated with the upwelling is also essential for the heat balance of the tropical Pacific Ocean. The heat input received at the surface is balanced by advection of cold water, but zonal advection does not achieve much in that respect in the tropics where the east-west temperature gradients are small. It is therefore mainly meridional advection and upwelling of colder subsurface water that balances the heat input.

In concluding the discussion of the equatorial current system it has to be pointed out that all its elements can change dramatically from one year to the next and that speeds and transports given above are therefore not necessarily representative for particular years. The variations are linked with the ENSO phenomenon which is the topic of Chapter 19. To give an idea of the changes that occur we only mention here that the EUC has been observed to disappear entirely for several months during the mature phase of an ENSO year, while the transport of the NECC increased to 70 Sv - twelve months later it was reduced to 2 Sv. Further discussion of these changes is postponed to Chapter 19.

The *Subtropical Countercurrents* in the region 20 - 26°N are also permanent features of geostrophic current calculations. They extend to the bottom of the thermocline and often to the 1500 m level. At the surface they can be found in ship drift data with speeds reaching 0.15 m s^{-1}. These eastward flows are located in the centre of the subtropical gyre and therefore not strictly part of the equatorial current system; but they are mentioned here for completeness. They do not exist east of the Hawaiian Islands and seem to be a modification of the Sverdrup circulation caused by the presence of that major barrier in the middle of the subtropical gyre - model calculations by White and Walker (1985) indicate that they would not exist if the Hawaiian archipelago were removed. However, banded current structure with alternating eastward and westward flow exceeding 0.5 m s^{-1} has also been reported from the region north of the Hawaiian Ridge (Talley and deSzoeke, 1986); so a final explanation remains to be developed. Similar subtropical countercurrents in the southern hemisphere can be expected from the Society Islands and the south Pacific islands further west.

Evidence for a South Subtropical Countercurrent in the Coral Sea was presented by Donguy and Henin (1975).

Western boundary currents

We begin the discussion of western boundary currents with the *Kuroshio* or "black (i.e. unproductive) current". All western boundary currents have a number of features in common: They flow as swift narrow streams along the western continental rise of ocean basins; they extend to great depth well below the thermocline; and they separate at some point and continue into the open ocean as narrow jets, developing instabilities along their paths. These features result from general hydrodynamic principles and reflect the balance of forces in the western boundary regions of the subtropical and subpolar gyres (the closure of the Sverdrup regime). Additional characteristics are imposed by the topography and give each boundary current its own individuality. The characteristic feature of the Kuroshio is that it has several quasi-stable paths. A complete description of the Kuroshio system therefore includes a number of alternative pathways (Figure 8.16). The current begins where the North Equatorial Current approaches the Philippines and continues northward east of Taiwan. It crosses the ridge that connects Taiwan with the Okinawa Islands and Kyushu and continues along the continental rise east of the East China Sea. As the ridge is less than 1000 m deep the current is relatively shallow in this region. It responds to the ridge crossing by forming the East China Sea meander. The meander shows some seasonality in strength and position, increasing in amplitude and moving northeastward in winter. Oscillations with periods of 10 - 20 days and wavelengths of 300 - 350 km occur along the Kuroshio front but the path along the East China Sea is quite stable otherwise. The Tsushima Current branches off from the Kuroshio near 30°N (see Chapter 10).

South of Kyushu the Kuroshio passes through Tokara Strait, a passage also not deeper than 1000 m, and bends sharply to the left. Downstream from Tokara Strait it has been observed near the 1000 - 1500 m isobaths to be only 600 m deep, with velocities above 1.0 m s^{-1} at the surface, 0.5 m s^{-1} near 400 m, and southwestward flow (i.e. opposed to the surface movement) of up to 0.2 m s^{-1} below. Geostrophic calculations indicate that even in 4000 m of water the current does not reach much beyond 1500 m depth. Further downstream along the continental rise of Japan the Izu Ridge south of Honshu forms another obstacle to the flow. The current negotiates it along one of three paths. In the "large meander" path the current turns southeastward near 135°E and flows northward along the ridge before crossing it close to the coast (path 3 in Figure 8.16). In the "no large meander" path it alternates between a path that follows the coast closely (path 1) and a small meander across the ridge (path 2). As shown in Figure 8.16 the change from paths 1 or 2 to the large meander situation occurs every few years at irregular intervals. During those years when the Kuroshio does not follow the large meander path the current changes between paths 1 and 2 about every 18 months. What causes the Kuroshio to change its path remains to be fully explained. Observations show a distinct increase in velocity before the current changes from the large meander path to paths 1 or 2. This suggests some kind of hydraulic control exerted by the Izu Ridge.

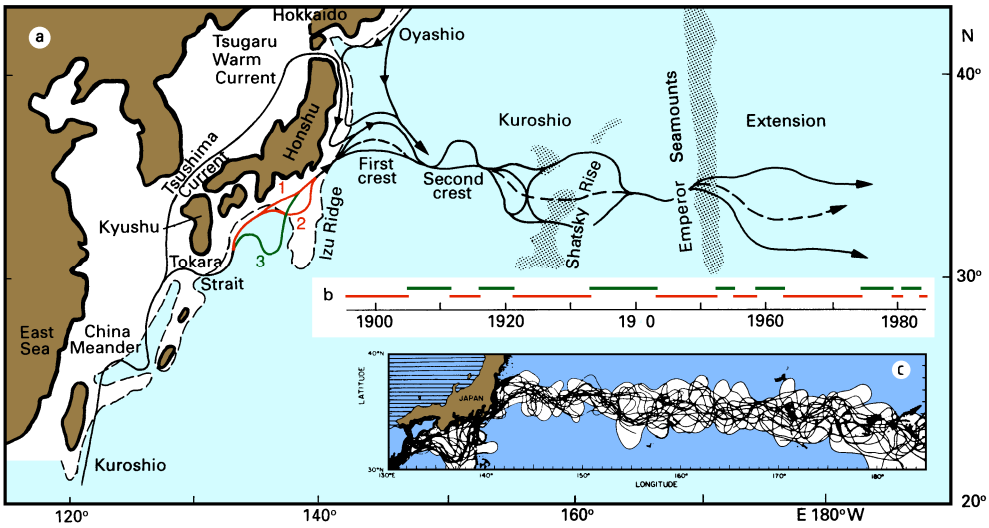

Fig. 8.16. Paths of the Kuroshio and Oyashio. (a) Mean positions of current axis, (b) time history of occurrence of the large meander path south of Japan (the current follows path 3 during the raised portions of the line), (c) individual Kuroshio paths observed during summer 1976 to spring 1980. The broken line is the 1000 m contour and indicates the shelf break. Adapted from Kawai (1972) and Mizuno and White (1983).

In the discussion of geostrophy in Chapter 3 we noted that rule 2 is valid in western boundary currents as long as the hydrographic section is taken across the current axis. The Kuroshio is thus linked with a dramatic rise of the thermocline towards the coast, and a horizontal temperature map at (for example) 300 m depth cuts through the oceanic thermocline near the Kuroshio axis (Figure 8.17). The position of the 15°C isotherm on the 300 m or 200 m level is commonly used as an indicator of the Kuroshio's position. When the temperature map is compared with maps of curl(τ/f) (Figure 4.3) it is seen that the region enclosed by the 15°C isotherm is a region of Ekman transport convergence (downwelling). Sinking motion in the surface layer removes nutrients and keeps biological productivity low despite high levels of sunlight. Ecologically, the central and western regions of the subtropical gyres are the oceanic equivalent of deserts. Devoid of detritus and other organic material, they display the deepest blue of all ocean waters and gave the Kuroshio (which carries their waters north) its name.

The separation point for the Kuroshio is reached near 35°N. It defines the transition from the Kuroshio proper to the Kuroshio Extension. Flow in the Extension is basically eastward, but the injection of a strong jet into the relatively quiescent open Pacific environment causes strong instability. Two regions of north-southward shift, the "First Crest" and the "Second Crest", are found between 140°E and 152°E with a node near 147°E. Both features, as well as the large meander path, are seen in the 300 m mean temperature (Figure 8.17) as features of the long-term mean circulation. East of the Second Crest the Shatsky Rise produces another region of alternative paths. On approaching the Emperor Seamounts the current breaks up into filaments which eventually form elements of the North Pacific Current.

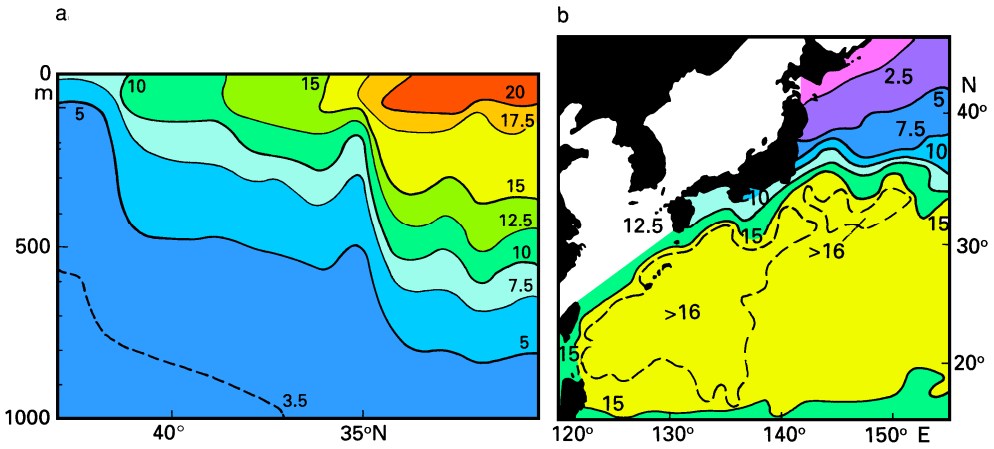

Fig. 8.17. The Kuroshio in the oceanic temperature field. (a) Vertical section of temperature (°C) across the Kuroshio Extension along 165°E, (b) temperature (°C) at 300 m depth. From Joyce (1987) and Stommel and Yoshida (1972).

Downstream from its separation point the Kuroshio continues into open water as a free inertial jet. Such jets create instabilities along their paths which develop into eddies or rings. In a map of eddy energy in the world ocean (Figure 4.8) the Kuroshio Extension therefore stands out as one of the regions with very high eddy energy. The process of ring formation is described in detail in Chapter 14 for the Gulf Stream, where more observations of the phenomenon are available. Kuroshio rings behave very much the same, so what is said in that chapter is relevant here as well. Observations over many years indicate that the Kuroshio forms about 5 rings every year when it flows along one of its stable paths and about 10 rings during years of transition. Kuroshio rings extend to great depth; analysis of long-term current meter measurements indicates coherence of kinetic energy virtually to the ocean floor. Eddy kinetic energy falls off across the Emperor Seamounts to one fifth of the amount observed in the west. Observations of deep flow over a one-year period (Schmitz, 1987) revealed unusually strong abyssal currents of 0.05 - 0.06 m s^{-1} below 4000 m depth just west of the Emperor Seamounts. These currents were directed westward near 165°E at either side of the Kuroshio Extension but eastward through a gap between two seamounts at 171°E, under the axis of the surface jet. The flow direction and strength was extremely stable and not reversed by eddies. In contrast, abyssal flow east of the Emperor Seamounts is so weak that it is regularly reversed by eddies, despite their lower energy levels there.

As in other western boundary currents, transport in the Kuroshio increases along its path, indicating entrainment of water from the subtropical gyre. In the Kuroshio Extension near 152°E and 165°E it has been estimated at 57 Sv, which is close to the 50 Sv estimated from closing the integrated Sverdrup flow. The current flows strongest during summer; seasonal variation of the sea level difference across Tokara Strait (0.6 m in the annual mean) indicates an increase of 13% from winter to summer. This apparently contradicts the

idea that the Kuroshio is the continuation of the North Equatorial Current, which reaches maximum flow in winter. However, the seasonal variation of the wind field and the associated Ekman pumping is not uniform across the tropical Pacific Ocean; and while the variation of NEC transport is in phase with the variation of the wind in the central region, the seasonal wind variation in the western region is in phase with the Kuroshio transport variation. This suggests that a significant part of the Kuroshio transport is wind-generated in the western Pacific Ocean.

North of its separation point the Kuroshio is opposed by the *Oyashio*, the western boundary current of the subpolar gyre. Ekman flow diverges in the centre of this gyre, so the Oyashio carries cold water rich in upwelled nutrients and full of marine life - hence its name the "parent current". The two mighty streams meet south of Hokkaido, where the *Tsugaru Warm Current* also brings water from the Japan Sea into the Pacific Ocean (as described in detail in Chapter 10). This water proceeds partly southward along Honshu, while another part moves eastward against the advance of the Oyashio. As a result the Oyashio generally splits into two paths, called the First and Second Oyashio Intrusion (Figure 8.16), and the region to the east of Tsugaru Strait displays extremely complicated hydrography (Figure 8.18). Between one and two anticyclonic (warm-core) eddies are formed each year in the region. Every six years or so one of them grows into a "giant eddy" which then dominates the area for nearly a year.

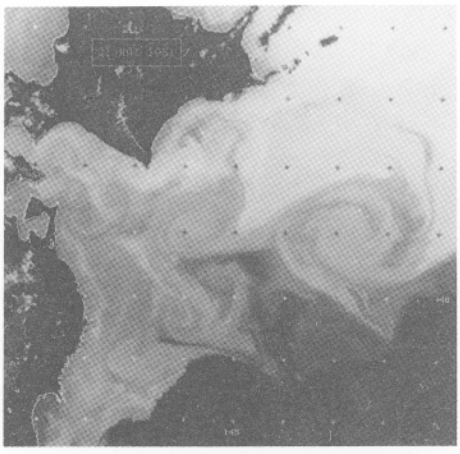

Fig. 8.18. Satellite image of sea surface temperature of the Kuroshio/Oyashio frontal region taken on 21 May 1981. The dark area in the southeast indicates very warm water in the Kuroshio. Warm water from the Tsugaru Warm Current enters from the west, through the channel between Honshu in the south and Hokkaido in the north; as indicated by the gray tones it proceeds southward along the Honshu coast. Light tones represent cold water of the Oyashio; the First Intrusion is indicated by the coldest water. A large anticyclonic (warm) eddy is centred at 41°N, 147°E. The Second Oyashio Intrusion is seen east of the eddy.

The complexity of the region is evident from the figure: Eddies, filaments, and meanders are seen in various stages of formation. In the centre of the observation area a jet-like intrusion from the Tsugaru Warm Current into Kuroshio water produces a "bipole", two small eddies of opposite rotation. (Bipoles are often found at straits or at outlets of strong-flowing rivers. Their eddies are smaller than eddies produced by western boundary currents and differ from them in that they contain the same water mass regardless of their sense of rotation - Kuroshio eddies contain warm water if they rotate anticyclonically but cold water if they have cyclonic rotation.) From Vastano and Bernstein (1984).

The southward boundary of the Oyashio with temperatures of 2 - 8°C defines the Polar Front; it is usually located at 39 - 40°N. Occasionally (for example during 1963, 1981, and 1984) the Oyashio pushes south as far as 36°N. This appears to occur when the region of zero wind stress curl moves southward, apparently extending the subpolar gyre southward by some 300 - 500 km. The southern edge of the Oyashio and the northern edge of the Kuroshio maintain their own frontal systems along the Kuroshio Extension. Thus, in the section shown in Figure 8.17a which is located about half-way between the Shatsky Rise and the Emperor Seamounts, the Kuroshio Front is seen at 35°N (identified by the 15°C isotherm) and the Oyashio or Polar Front at 41°N (the 5°C isotherm). The two fronts are associated with geostrophic flow, the front at 35°N with the 57 Sv of the Kuroshio and the front at 41°N with another 22 Sv as the continuation of the Oyashio. Between the two flows and on either side movement is weakly westward.

The Oyashio is the continuation of two currents. The *Kamchatka Current* brings water from the Bering Sea southward. It is associated with quasi-permanent anticyclonic eddies on the inshore side which are caused by bottom topography and coastline configuration and result in countercurrents along the coast. The larger of the two Oyashio sources is the *Alaskan Stream*, the extension of the western boundary current along the Aleutian Islands. The distinction between the Alaskan Stream and the Alaska Current further to the east is gradual, and the two currents are sometimes regarded as one. They are, however, of different character, the Alaska Current being shallow and highly variable but the Alaskan Stream reaching to the ocean floor. This indicates that despite its relatively modest speed of 0.2 - 0.3 m s^{-1} the latter is a product of western boundary dynamics, while the former belongs to the eastern boundary regime.

No transport estimates are available for the Alaskan Stream over its entire depth. Geostrophic estimates for the transport in the upper kilometer in the region 155 - 175°W vary between 5 and 12 Sv and show a width of the Stream of 150 - 200 km (Royer and Emery, 1987). South of the Stream the *North Pacific Current* continues from the Kuroshio and Oyashio Extension through the region between 30°N and some 200 km off the Alaskan coast, a broad band of eastward flow more than 2000 km wide. Because of the heavy distortion of distances in the subpolar parts of Figure 8.6, the figure cannot adequately portray this difference in width. Some authors distinguish between the North Pacific Current as the continuation of the Kuroshio Extension south of about 43°N and a Pacific Subarctic Current to the north representing the continuation of the Oyashio Front. Whether the clear separation of the Kuroshio and Oyashio Fronts in the west is maintained all across the Pacific basin, effectively suppressing exchange of water between the subtropical and subpolar gyres, is doubtful, and it appears more appropriate to regard all eastward flow south of Alaska part of the same broad current.

A prominent western boundary current of the equatorial current system is the *Mindanao Eddy*. Captains of vessels that carry Australian wealth to Japan know it well and take advantage of it by following the Mindanao coast southward on their way from Japan to western Australia while travelling 100 - 200 km offshore on their way north. Its transport is estimated at between 25 and 35 Sv, with strong interannual variations. Observations in the western part of the eddy (the *Mindanao Current*) show that the equatorward flow does not extend below 250 m; flow in the depth range 250 - 500 m is poleward and carries some 16 - 18 Sv. The *Halmahera Eddy* and the *New Guinea Coastal Current* are seasonal boundary currents near the surface (the latter flows northwestward throughout the year below 200 m, see Fig. 8.11). The flow direction shown in Figure 8.6 reverses during a few

months when the region of the Philippines, New Guinea, and northern Australia experiences the monsoon of the southern summer season: from December to March winds over the Philippines blow from the northeast, and from the northwest south of the equator (Figures 1.2b and c).

The *East Australian Current* is the western boundary current of the southern hemisphere. Although it is the weakest of all western boundary currents, carrying only about 15 Sv in the annual mean near 30°S, it is associated with strong instabilities. Its low transport volume is partly a consequence of flow through the Australasian Mediterranean Sea; models show that if the Indonesian passage were closed, flow from the Pacific into the Indian

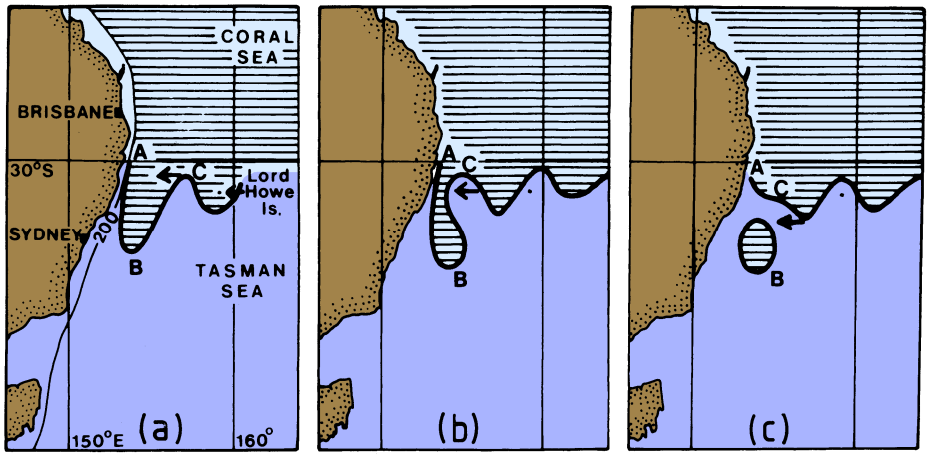

Fig. 8.19 (above). A sketch of eddy formation in the East Australian Current through Rossby wave propagation along the Tasman Front. Point *C* moves westward towards *A*. In the process it pinches off the meander and releases current ring *B* which moves southward. Shading indicates warm Coral Sea water. From Nilsson and Cresswell (1981).

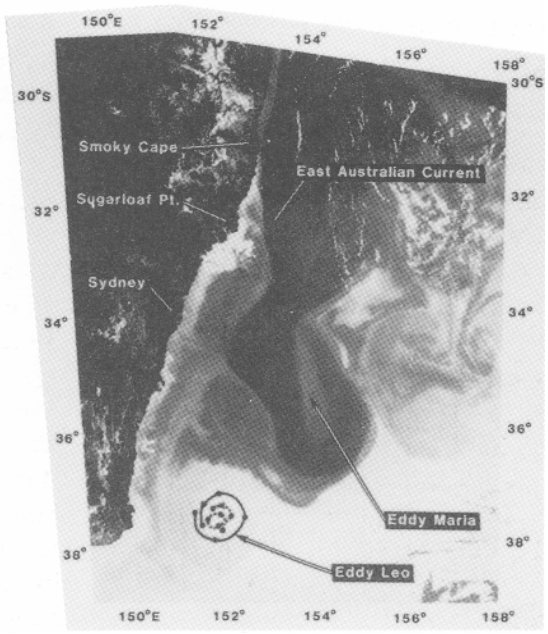

Fig. 8.20 (left). The East Australian Current seen in the sea surface temperature distribution as observed by satellite on 20 December 1980. Dark is warm, light is cold. (Some small scale very light features are clouds.) The tracks in eddy "Leo" are the paths of two drifting buoys. Dots indicate noon positions for each day. From Cresswell and Legeckis (1986).

Ocean would be diverted through the Great Australian Bight, doubling the transport of the East Australian Current. The instabilities may result in part from the fact that the current first follows the Australian coast but has to leave it to continue along the eastern coast of New Zealand. The current therefore separates from the Australian coast somewhere near 34°S (the latitude of the northern end of New Zealand's North Island). The path of the current from Australia to New Zealand is known as the Tasman Front, which marks the boundary between the warm water of the Coral Sea and the colder water of the Tasman Sea. This front develops wave-like disturbances (meanders) and associated disturbances in the thermocline which eventually travel westward with Rossby wave speed. When the waves impinge upon the Australian coast they separate from the main current and turn into eddies.

Figure 8.19 shows the process of eddy formation. Because the meander closest to the coast always extends southward and thus can trap water only from the Coral Sea, the East Australian Current spawns many anticyclonic (warm core) but few cyclonic (cold core) eddies. Figure 8.20 shows the current extending to 37°S, flowing back past 34°S before turning eastward and forming the warm eddy "Maria" in the process. A band or "ring" of warm water is clearly seen around the eddy, indicating the region of strongest currents. When the eddy becomes separated from the main current it will maintain its speed (1.5 - 2.0 m s^{-1}) for many months while its hydrographic structure changes. Eddies that go through winter cooling and subsequent spring warming lose their surface signature and are no longer detectable in satellite observations of sea surface temperature (Figure 8.21). Eddy "Leo" in Figure 8.20 is such an eddy; its presence is revealed by the track of two drifting buoys but not visible in the temperature pattern. Remnants of eddies in the form of subsurface layers of uniform temperature and salinity are abundant south of the Tasman Front and are characteristic of the upper 500 m of the Tasman Sea (Figure 8.22).

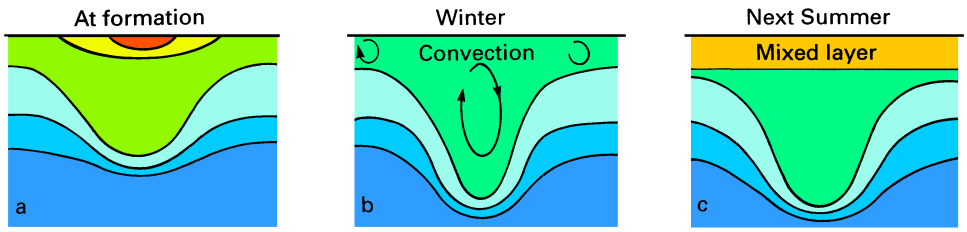

Fig. 8.21. Evolution of the hydrographic structure in an East Australian Current eddy: isotherms in a section across the eddy (a) at the time of formation, (b) during winter, (c) in the following summer. The original warm ring signature at the surface is destroyed by convection from cooling in winter. The eddy is then capped by the seasonal thermocline in the following spring.

The East Australian Current spawns about three eddies per year, and some 4 - 8 eddies may co-exist at any particular time. Because the volume transport in the current is low, the eddies can contain more energy than the current itself. On occasions it is impossible to identify the path of the current; the western boundary current system then is a region of intense eddy activity without well defined mean transport. This is particularly true for the passage of the current from Australia to New Zealand, where an average location of the

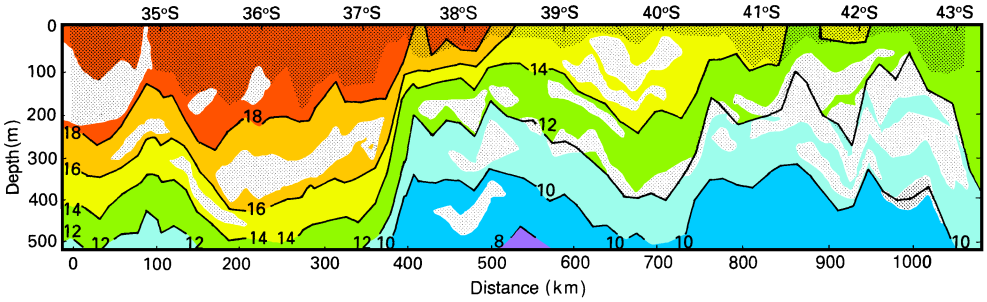

Fig. 8.22. A section of temperature (°C) through the Tasman Sea along a track about 150 km seaward of the continental shelf. The shaded regions indicate layers where the temperature changes by less than 0.1°C. In the permanent thermocline where the temperature usually changes by 0.1°C every 5 m, such layers indicate remnants of cores from East Australian Current eddies. From Nilsson and Cresswell (1981).

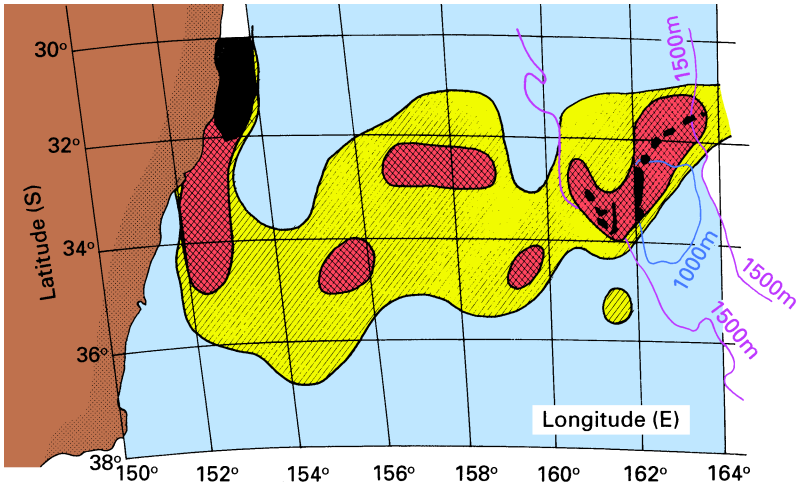

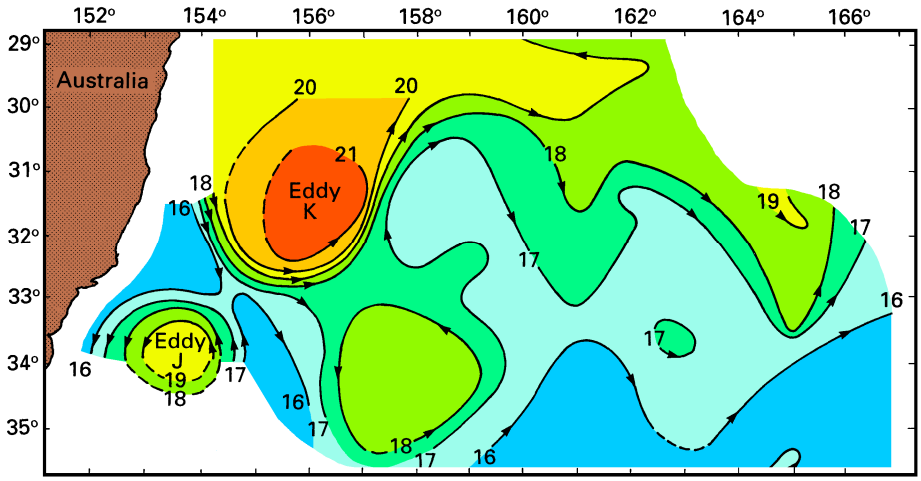

Tasman Front can only be defined in statistical terms (Figure 8.23). The current is stronger and reaches further inshore in summer (December - March) than in winter. This is evident from ship drift reports obtained from vessels sailing along the Australian coast between Bass Strait and the Coral Sea. These ships take advantage of the East Australian Current by proceeding along the shelf break on their voyage south; northbound vessels stay inshore of the Current and remain over the shelf. Figure 8.24 shows that during winter northbound vessels occasionally experience an inshore countercurrent to assist their voyage. In summer they may encounter southward flow of more than 1 m s^{-1} even on the shelf.

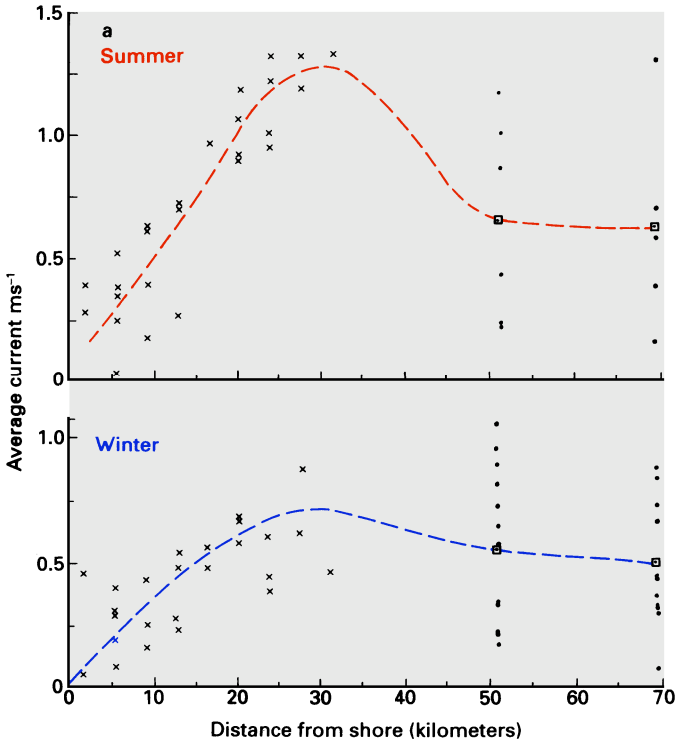

Fig. 8.24. Seasonal variability of the East Australian Current. (a) Mean current velocity for summer and winter near 30°S. See page 130 for part b of the figure. From Godfrey (1973) and Hamon *et al*. (1975).

Fig. 8.23 (page 128). The Tasman Front. Top: Dynamic topography (m^2 s^{-2}), or steric height multiplied by gravity, as observed in September - October 1979, showing the Tasman Front as a band of large steric height change along the 18 m^2 s^{-2} contour; to obtain approximate steric height in m, divide contour values by 10. Bottom: Mean position of the front as determined from satellite SST observations during March 1982 - April 1985; the front was found during more than 30% of the observation period in the lightly shaded area, more than 50% of the time in the dark region, and always in the black region. Adapted from Stanton (1981) and Mulhearn (1987).

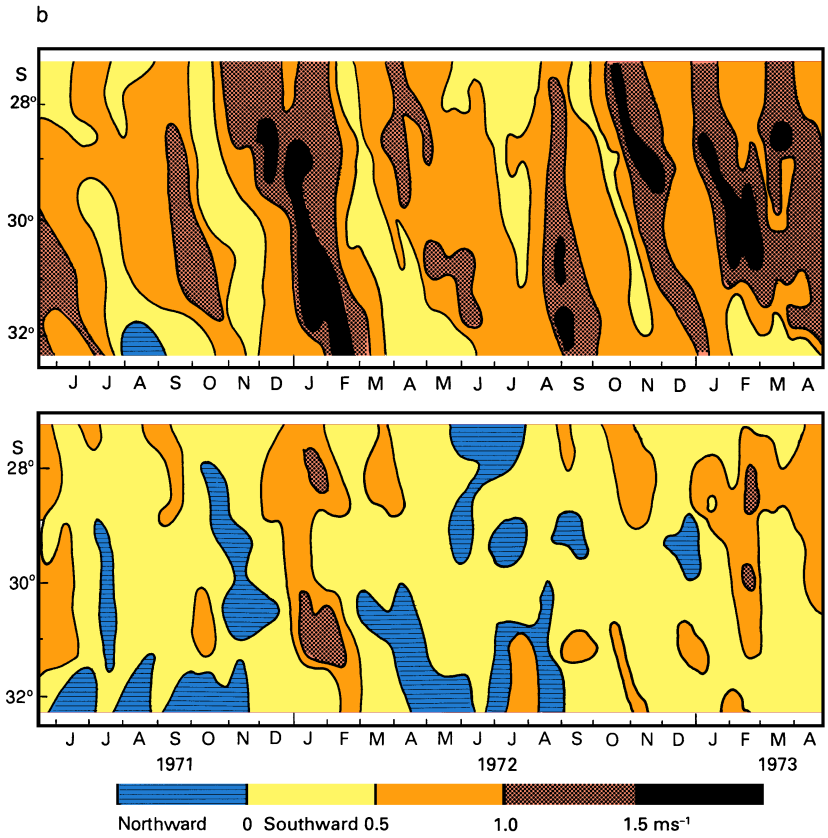

Figure 8.24 (continued). b) current velocity deduced from the drift of southbound vessels (top; mean offshore distance 19 km) and from the drift of northbound vessels (bottom; mean offshore distance 6.5 km) as a function of time. From Godfrey (1973) and Hamon *et al.* (1975). See page 129 for part a of the figure.

The continuation of the East Australian Current east of New Zealand is the *East Auckland Current*. It forms an anti-cyclonic eddy north of East Cape (near 37°S) similar in size and with the same homogeneous deep core as the eddies in the Tasman Sea; the eddy is, however, apparently topographically controlled, being found at the same location throughout the year. There is evidence that the East Auckland Current undergoes seasonal change; during summer most of its transport continues as the *East Cape Current* and follows the New Zealand shelf southward until it reaches the Chatham Rise, while during winter some of it separates from the shelf and continues zonally into the open ocean, forming a temperature front near 29°S. Another shallow front near 25°S, sometimes referred to as the Tropical Front, marks the northern limit of eastward flow in the subtropical gyre. At the surface, the westward flow of the South Equatorial Current rarely extends more than 300 km to the south of Fiji (i.e. 20°S); but the boundary between eastward and westward flow slopes down to the south, and at 800 m depth it is found more at 30°S (Roemmich and Cornuelle, 1990).

Eastern boundary currents and coastal upwelling

In the vertically integrated flow, the eastern part of the Pacific Ocean occurs as a region of broad and weak recirculation for the ocean-wide gyres. This is correct for the mean flow away from coastal boundaries but does not hold for currents over short periods and close to the shelf. The aspect of short term variability in the open ocean was already addressed through an example from the Atlantic Ocean (Figure 4.9); the same arguments apply to the Pacific or Indian Oceans. Closer to shore the dynamics are further modified as a result of the meridional direction of the winds. To understand the resulting circulation, known as coastal upwelling, it is necessary to review very briefly the balance of forces along eastern ocean boundaries.

The reason for the strong equatorward component of the Trades along eastern ocean coastlines is the strong difference in climatic conditions between the eastern and western coasts. In the west the Trades impinge on the land laden with moisture which they collected from evaporation over the sea. The coastal regions are therefore well supplied with rainfall; the eastern coastal regions of Madagascar, Brazil, Southeast Asia, New Guinea and the Cape York peninsula of Australia are all covered with luxurious rainforest. At the same latitudes in the east the Trades arrive depleted of moisture, having rained out over the land further east. Lacking the essential rain the coastal regions are deserts: the Simpson desert in Australia, the Atacama desert in South America, the Namib in South Africa, and the Californian desert regions in North America are all found at the same latitudes where rainforests flourish on the opposite side of the oceans. Over these desert lands the air is dry and hot in summer, creating low pressure cells (Figure 1.3). The resulting pressure difference between land and ocean gives rise to equatorward winds along the coast.

The effect of the wind on the oceanic circulation was already demonstrated in Figure 4.1 and is described in more detail in Figure 8.25: The Ekman transport E produced by equatorward winds is directed offshore; as a result the sea surface is lowered at the coast. The corresponding zonal pressure gradient which develops in a band of about 100 km width along the coast supports a geostrophic flow GF toward the equator, i.e. in the same direction as the wind. The water that is removed from the coast at the surface has to be supplied from below, hence upward water movement (of a few meters per week) occurs in a narrow region close to the coast. This upwelling water in turn has to be supplied from the offshore region. On a shallow shelf this can occur in a bottom boundary layer as indicated in Figure 8.25b, but outside the shelf flow toward the coast has to be geostrophic. In other words, in addition to the zonal pressure gradient produced by the Ekman transport, a meridional pressure gradient must exist as well, to support the supply of water for the upwelling process. This pressure gradient is directed poleward; geostrophy implies that it is balanced by the Coriolis force linked with the onshore water movement. Close to the coast this movement runs into the shelf and comes to a halt, the associated Coriolis force goes to zero, and we encounter a situation already familiar from the dynamics of the Equatorial Undercurrent: In the absence of an opposing force the pressure field accelerates the water down the pressure gradient, until frictional forces are large enough to prevent further growth of the velocity. The result is poleward flow PF in a narrow band near and above the shelf break. This flow competes with the equatorward geostrophic flow driven by the zonal pressure gradient. It is therefore usually not observed at the surface but always seen as an undercurrent along the continental slope. Note that similar to western boundary currents or the equatorial undercurrent only the downstream pressure gradient is not in geostrophic

balance. The cross-stream pressure gradient adjusts itself to geostrophic balance with the undercurrent, which can therefore be seen in a downward tilt of the isotherms and isohalines toward the shelf below the surface layer. At the surface, the upward tilt of the isotherms and eventual surfacing of the thermocline gives rise to a front which, through geostrophic adjustment, produces an intensification of the flow known as the coastal jet *CJ*.

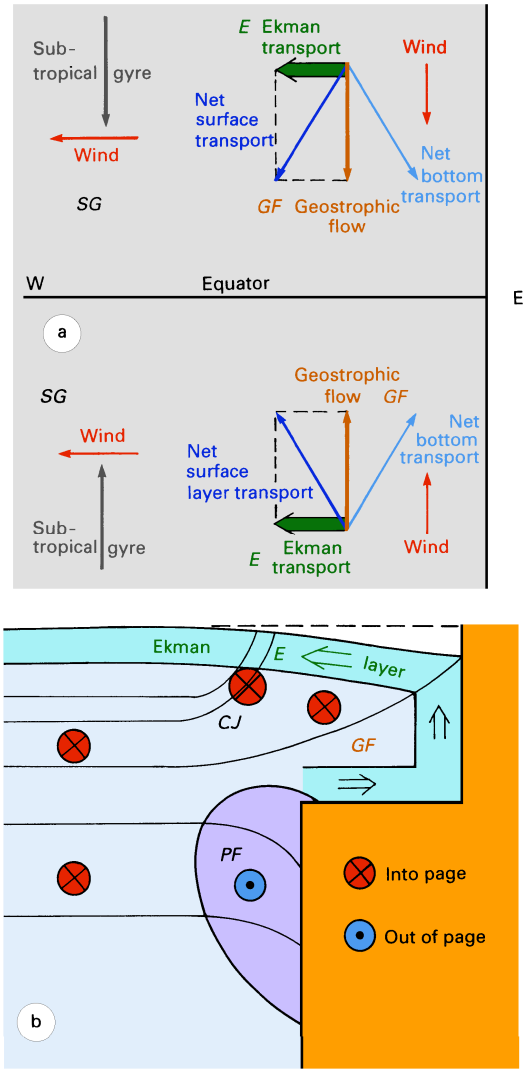

Fig. 8.25. Dynamics of coastal upwelling regions.

(a) plan view,

(b) vertical section (southern hemisphere).

The thin lines in (b) represent isotherms or isopycnals. See text for details.

The upwelling circulation just described is embedded in the much broader equatorward flow of the subtropical gyre circulation *SG*. At the surface the two circulation systems combine to advect cold water towards the tropics, lowering the sea surface temperature along the eastern boundary. The result is a deflection of isotherms from zonal to meridional

orientation along the eastern boundary (Figure 2.5a). The water warms as it moves equatorward and offshore; this is reflected in large net heat fluxes into the ocean (Figure 1.6).

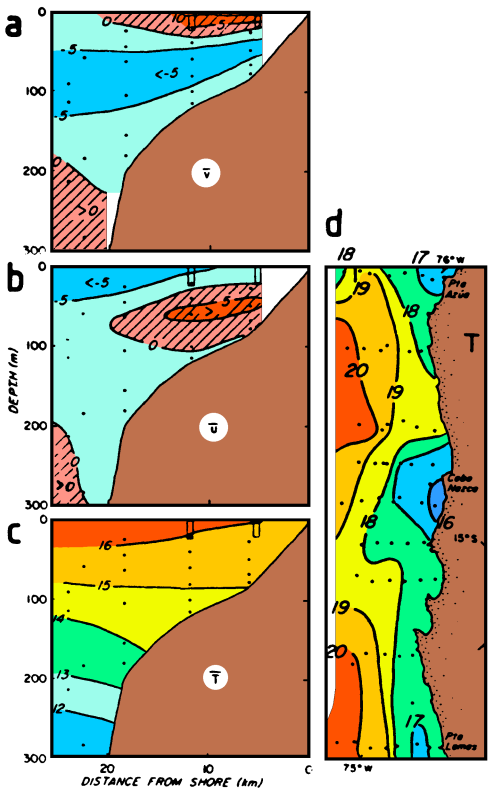

Fig. 8.26. The Peru/Chile upwelling system. (a) Mean alongshore velocity (cm s^{-1}, positive is equatorward), (b) mean cross-shelf velocity (cm s^{-1}, positive is shoreward); the offshore Ekman transport is indicated by negative values in the surface layer), (c) mean temperature (°C); all means are for the period 22/3 - 10/5/1977. Dots indicate current meters, the blocks at the surface special moorings. (d) Sea surface temperature during 20 - 23/3/1977. From Brink *et al.* (1983).

The most impressive coastal upwelling system of the world ocean is found in the *Peru/Chile Current*. This current is strong enough to lower sea surface temperatures along South America by several degrees from the zonal average (Figure 2.5a). Embedded in the current is a vigorous upwelling circulation which lowers the temperatures within 100 km of the coast by another 2 - 4°C. The coastal upwelling band is too narrow to be resolved by the ocean-wide distribution of Figure 2.5a, so the low temperatures seen on the oceanic scale reflect advection of temperate water in the subtropical gyre. To see the effects of the coastal upwelling circulation we have to take a closer look at the inshore region. Figure 8.26 shows equatorward surface flow above 30 m, the poleward undercurrent between 30 m and 200 m, offshore Ekman transport above 30 m, and onshore movement of water mainly in the range 30 - 100 m with very little onshore or offshore movement below. Onshore transport in coastal upwelling regions does not extend below 400 m at most. The depth range for onshore movement in the Peru/Chile upwelling system is, however, particularly shallow, probably as a result of the extreme narrowness of the shelf. Upwelling is indicated by the shoaling of the 16°C isotherm, while the downward slope

toward the coast of the isotherms below 100 m indicates geostrophic adjustment of the density field to the undercurrent along the slope.

Coastal upwelling systems are among the most important fishing regions of the world ocean because they offer optimum conditions for primary production. The basis for all marine life is photosynthesis in phytoplankton, which can only occur in a layer as deep as sunlight can reach (the so-called euphotic zone, which is less than 200 m deep even in very clear water and usually much shallower). The other requirement are nutrients to support phytoplankton growth. They are supplied by remineralization of dead organisms. In contrast to the nutrient cycle on land, where dead organisms are composted and the nutrients returned to the soil, the nutrient cycle in the open ocean is not very efficient: Much of the nutrient reservoir is locked below the euphotic zone because dead organisms sink and escape from the euphotic zone before they can be remineralized. Coastal upwelling regions are among the few regions of the world ocean where nutrients are returned to the surface layer and made available for phytoplankton growth. This forms the basis for a marine food chain with high productivity. All coastal upwelling regions therefore support important fisheries.

The Peru/Chile upwelling system is the most productive coastal upwelling region of the world ocean. It extends from south of 40°S into the equatorial region where it blends into the equatorial upwelling belt. Despite its vast resources, human greed managed to destroy the basis of what before 1973 was the largest fishery in the world. Overfishing and natural variability of the upwelling environment brought about the end of an industry. This aspect of the Peru/Chile Current System will be taken up again in Chapter 19.

Considerable uncertainty exists about the details of the flow field in the southern part of the Peru/Chile Current. The upwelling undercurrent is known to extend from at least north of 10°S to 43°S and possibly beyond, decreasing in strength from some 0.1 m s^{-1} in the north to barely more than 0.02 m s^{-1} in the south. Further offshore a conspicuous feature is a surface salinity minimum along 40°S (Figure 2.5b). It is known that rainfall along the coast is large in the region; but it can easily be shown that rainfall alone cannot explain the observed salinity minimum. Some researchers conclude that westward flow against the prevailing direction of the subtropical gyre circulation must occur in the region. This may explain why the Subtropical Front is displaced so far northward in the Pacific Ocean off South America and ill defined.

The corresponding coastal upwelling region in the northern hemisphere is found in the *California Current*. Its vast living resources are known from John Steinbeck's novel "Cannery Row" set in Monterey, the centre of the sardine fishery before it collapsed from overfishing in the 1930s. Winds along the coast are much more seasonal here than along the coasts of Peru and Chile (Figure 1.2). Equatorward winds prevail along the coast of Washington, Oregon, and California from April into September, while during the remainder of the year winds are variable and often southeasterly. As a result, poleward flow at the surface is observed during October - March over the shelf and even further offshore. This seasonal flow, which reaches its peak with 0.2 - 0.3 m s^{-1} in January - February, is often called the *Davidson Current*. Coastal upwelling with equatorward surface flow prevails during spring and summer, lowering the sea surface temperatures along the coast to 15°C and less at a time when only kilometres away the heat on land is hardly bearable. The associated cooling of the air leads to condensation, and a coastal strip usually less than a kilometer wide is nearly permanently shrouded in sea fog - the postcard photographs of the famous Golden Gate bridge spanning a blue San Francisco Bay in bright sunshine cannot

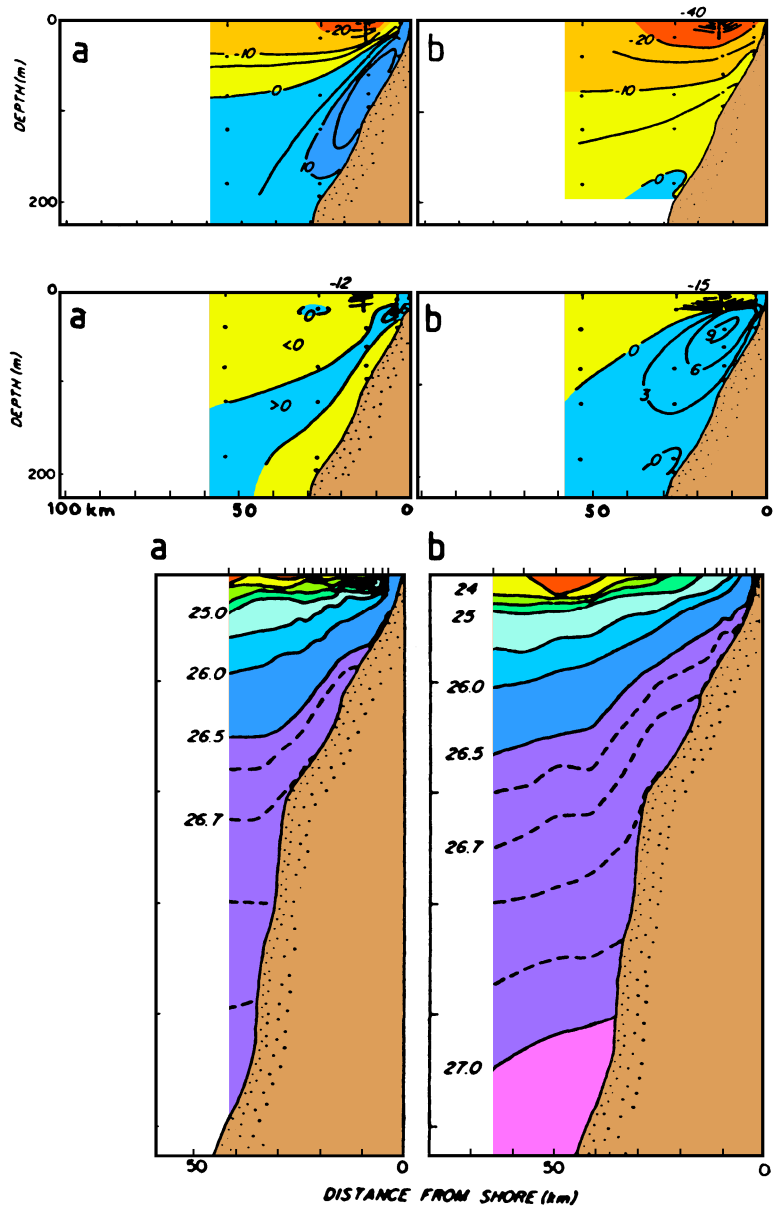

Fig. 8.27. Alongshore flow v (top; cm s^{-1}, positive is poleward), cross-shelf flow u (middle; cm s^{-1}, positive is shoreward), and density σ_t (bottom) in the Californian upwelling system. Left: During weak wind conditions, right: during strong wind conditions. Intensification of upwelling during strong winds is indicated by an increase in u and an increase in equatorward flow accompanied by a reduced undercurrent. The shallow pycnocline (near $\sigma_t = 24.5$) breaks the surface, forming a front some 20 km offshore during periods of strong upwelling; when the wind relaxes this front recedes towards the coast and may eventually disappear. From Huyer (1976).

be taken until October when the upwelling ends and sea surface temperatures reach their annual maximum. Even during the upwelling season poleward flow prevails along the coast of southern and central California in an inshore strip of up to 100 km width, apparently as part of a large cyclonic eddy between the California Current and the coast which has been observed to exist throughout the year except during March and April. Further north, inshore poleward flow with velocities in excess of 0.3 m s^{-1} can exist during periods of weak winds but is suppressed if the upwelling is strong.

High variability of winds and upwelling intensity are a characteristic feature of the Californian upwelling system. Figure 8.27 shows the circulation during a period of weak wind and a period where winds were particularly strong. The competing influences of wind-driven equatorward flow and poleward flow driven by the alongshore pressure gradient are seen in the weakening of the undercurrent as the wind increases.

North of the Californian upwelling region is the *Alaska Current*, also called the Alaska Coastal Current, the eastern component of the subpolar gyre. Freshwater input from Alaska's rivers reduces the density in the upper layers near the coast, enhancing the pressure gradient across the current and constraining the current path to the coastal region. As a consequence, the current is concentrated on the shelf. It is strongest in winter when it shows speeds of up to 0.3 m s^{-1} and weakest in July - August when the wind tends to oppose its flow (Figure 1.2). During some years flow east of 145°W ceases altogether during these months and the subtropical gyre is displaced some 700 km westward (Royer and Emery, 1987). Eddies may then dominate the region along the Canadian/Alaskan coast. A well defined anticyclonic eddy has been reported from buoy tracks and cruise data off Sitka (Figure 8.28) with average surface speeds exceeding 0.7 m s^{-1}. The eddy exists during spring and summer and possibly throughout the year. It reaches to at least 1000 m depth, although its speed is reduced by half at 200 m.

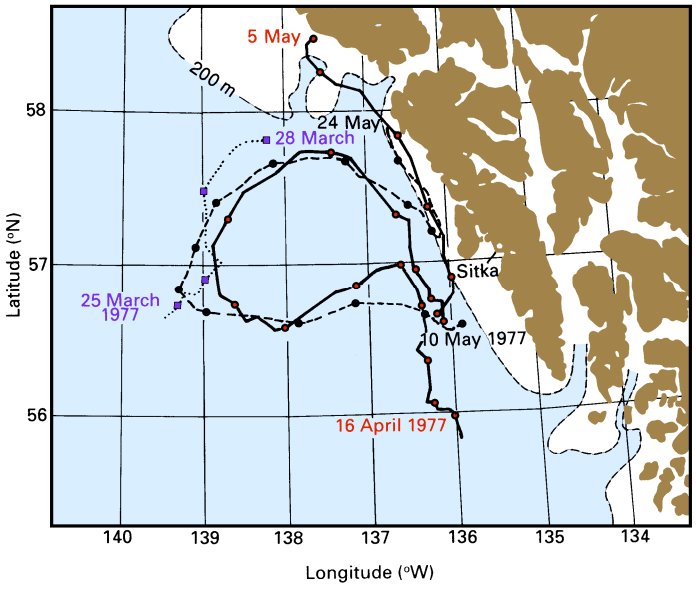

Fig. 8.28. The anticyclonic eddy off Sitka as seen in the trajectories of three satellite-tracked buoys during March - May 1977. From Tabata (1982).